

**Exploring Spatial and Temporal Differences Between High and Low Frequency Water  
Quality Data in Coastal Virginia**

Emma Brahmey  
Fairfax, Virginia

B.A., University of Virginia, 2021

A Thesis presented to the Graduate Faculty  
Of the University of Virginia in Candidacy for the Degree of  
Master of Science

Department of Environmental Sciences

University of Virginia  
April 4th, 2023

**Abstract**

In coastal Virginia, water quality variables such as temperature, salinity, dissolved oxygen (DO), chlorophyll-a (Chl), and apparent oxygen utilization (AOU) are important biogeochemical measures of water status. Accurate monitoring and modeling of these variables is vital in order to characterize the processes driving seasonal and geographic patterns. Using harmonic analysis, a method that fits sine and cosine functions to seasonally varying data, I investigated the differences in the date and value of minimum/maximum observations as well as seasonal amplitudes for the respective water quality variable on spatial and temporal scales. High and low frequency monitoring sites provide contrasting cases for harmonic analysis and for investigation of storm impacts on coastal water quality anomalies. On both time and space scales, subsampled short term high frequency (4-6 years of 15 minute resolution) inland sites were compared to long term low frequency (30 years of quarterly sampled resolution) environmentally variable water quality sites on the Eastern Shore of Virginia. Strong seasonal patterns were observed, with all sites being dominated by the first harmonic for temperature, DO, and AOU, and a mix of first and second harmonic dominating for salinity and Chl. Long term changes in temperature, salinity, Chl, and AOU were found in many of the sites. Specifically at high frequency sites, simulated quarterly sampling was performed and error variability was calculated between the successive years of subsampled and full model values using logarithmic regression. Above 25 years was found to be the ideal time period of low frequency monitoring to limit the year to year variability in error, with 50 years reaching a plateau in this error. This analysis provided an understanding of baseline seasonal patterns as well as anomalies. Diurnal anomalies were examined in both magnitude and directional changes due to weather factors based on a storm and seasonal scale. Correlations with water quality variables were seen across

all seasons and storm types, with temperature, salinity, DO, and Chl being the most frequent with water level anomalies and precipitation. These correlations related to disturbances may become more severe and/or frequent as the amount and severity of storms and flooding increase due to global warming and sea level rise.

## **Acknowledgements**

I would like to thank my advisor Scott Doney and committee members Karen McGlathery and Mike Pace for their guidance throughout my graduate career and thesis process.

Also thank you to the Doney Lab, especially Joy Ferenbaugh, Carly LaRoche, and Mary Stack, for their unwavering support, advice, and friendship throughout the last two years.

Finally, thank you to my family for all the love and emotional support throughout my time at UVA. I would not have finished my thesis without them, and am very grateful.

**Table of Contents**

<u>Section</u>	<u>Page</u>
1. Introduction	1
2. Literature Review	4
2.1 The Importance of Selected Water Quality Variables	4
2.2 High Frequency vs Low Frequency Water Quality Monitoring	7
2.3 Relationship between storm events and water quality	8
3. Research Questions	9
4. Methods	10
4.1 Site and Data Descriptions	10
4.2 Data Analysis	13
5. Results and Discussion	20
5.1 High vs Low Frequency Seasonal Harmonic Analysis	20
5.2 Seasonal High Frequency Anomaly Analysis	36
5.3 Storm Event High Frequency Anomaly Analysis	39
6. Summary	44
7. Conclusions and Future Directions	46
8. Appendix	48
9. References	58

## 1. Introduction

Coastal lagoons are water bodies enclosed seaward by barrier islands and downstream of coastal rivers and creeks landward (Scanes et al., 2007). They are usually shallow with submerged, often vegetated flats and intermittent openings to the sea (Scanes et al., 2007). Lagoons include or are adjacent to important habitats such as wetlands, mangroves, salt-marshes, and seagrass meadows that host high biodiversity and provide services such as fishing, freshwater storage, hydrological balance, climate regulation, flood protection, water purification, oxygen production, recreation and ecotourism (Newton et al., 2018). Lagoon water quality is influenced greatly by evaporation, precipitation, groundwater input, surface runoff, and exchange with the ocean (Anthony et al., 2009). However, they are vulnerable to water quality degradation due to habitat destruction, pollution, water withdrawal, overexploitation, and invasive species, as well as the rising threat of climate change (Newton et al., 2018).

The coastal Virginia lagoon system is very specific, as it is the largest expanse of undeveloped coastline that is rural, allowing for higher water quality, especially low nutrient loading and water column chlorophyll concentrations (Carr et al., 2012). It also lacks significant inputs of fluvial sources of freshwater and sediment (Safak et al., 2015), and due to the lack of riverine input its salinity varies very little from that of full marine salinity (Oreska, 2021). It historically hosted large scallop fisheries due to the abundance of *Zostera marina* seagrass beds until a massive dieoff event in the 1930s (Hondula & Pace, 2014). Due to large scale restoration efforts, reseeded has allowed for 4000 acres of beds to return as of 2014 (Hondula & Pace, 2014). In this area, climate is the most dominant driver of ecological change, especially sea level rise, storms, and higher temperature shifts (*VCR/LTER Proposal 2018*, 2018). The water quality varies as a function of season, current, wind, and storm conditions (Hondula & Pace, 2014). The

Virginia Coast Reserve (VCR) houses 13 long term low frequency water quality monitoring sites on the Eastern Shore of Virginia with varying site types, water depths, and residence times (Safak et al., 2018). Most of these sites are relatively shallow (1-2 m MSL) and oligotrophic, with a mean semi-diurnal tidal range of 1.2 m (Oreska et al., 2021). The Virginia Institute of Marine Science (VIMS) at the Eastern Shore Laboratory (ESL) houses 2 shorter term high frequency water quality monitoring sites that are both inland.

Water quality is an important metric of measuring the status of bodies of water, especially variables such as temperature, salinity, dissolved oxygen (DO), apparent oxygen (AOU), and Chlorophyll-a (Chl). These measures tell important information about the biogeochemical properties of the system, and are likely to experience significant changes due to climate change. They are also highly interconnected, for example warming water temperatures can allow for algal blooms (elevated levels of Chl), which can lead to the formation of hypoxic and anoxic zones (low to no DO), which in turn can influence the community metabolism (AOU which depends on temperature, salinity, and observed DO values).

Establishing consistent and adequate water quality monitoring is essential to protecting these areas. High frequency monitoring collects *in-situ* measurements using automated sondes that are able to collect at a high temporal frequency (for example every 15 minutes) without the time intensive labor needed for manual collection. However, these are mostly confined to shore based sites due to power demands and subject to sensor malfunction with consequent loss of consistent time series. Low frequency monitoring is collected using a manual sonde and lab extraction methods and has a lower temporal frequency (monthly to quarterly). It is limited by both labor costs and availability, as well as being restricted to good weather conditions.

However, in coastal Virginia these data sets have the advantage of longer data availability and more sites with higher geographic spread, as well as being less prone to sensor malfunction.

Modeling seasonal patterns can be accomplished using harmonic analysis, a method that represents fluctuations in a time series from the sum of sine and cosine functions that have different time periods (or frequencies) (Wilks, 2011). This method can accommodate gaps in the data as well as being applicable for multi-year analysis, making it ideal for both high and low frequencies of water quality collection. Higher harmonics indicate higher frequencies, with the first harmonic (also called the fundamental harmonic) representing the full cycle completed in the designated period of time, one year in terms of seasonal data, indicating an annual cycle (Wilks, 2011). The second harmonic indicates two full cycles within the year time frame, a semi-annual cycle with seasonal data. Higher harmonics can be computed, however for this project only the first and second harmonics were calculated to make comparisons between variables efficiently. The relative importance of each of these harmonics can be quantified using their respective variances, with a larger variance correlating with a greater importance. Most variables have their variance captured by these first two harmonics. For example, the first harmonic accounts for 90% or more of the total seasonal variance for water temperatures (Kothandaraman & Evans, 1972). A composite harmonic, the addition of the first and second harmonic, allows for the relative importance of each harmonic to be seen in the resulting curve and elements. For example, a harmonic curve with 90% first harmonic and 10% second harmonic, would look almost identical to the first harmonic, while a harmonic curve with 45% first harmonic and 55% second harmonic would have elements of both.

Harmonic elements such as amplitude, phase shift and minimum/maximum values can reveal important information about seasonal cycles. The phase shift indicates the location in the

curve of the peak value, and can be expressed as day of year to highlight when the maximum occurs. The minimum/maximum value indicates the most extreme value in the cycle, and the seasonal amplitude quantifies the difference between them divided by two. These values are easy to compare between both sites and frequencies. To account for more data availability in high frequency sites, during comparisons with low frequency sites random subsampling methods can be used in order to get an average harmonic fit and elements with confidence intervals via bootstrapping.

Deviations from day of year harmonic fits can indicate anomalies, also known as deseasonalized data, which allow for documentation of trends in long term data. These anomalies on a diurnal scale can also be investigated to see if there are seasonal or weather based events that can account for very high magnitude values using methods such as Generalized Least Squares (GLS) at high frequency sites.

## **2. Literature Review**

### **2.1 The Importance of Selected Water Quality Variables**

Water quality is a vital way to monitor bodies of water in changing climate conditions. Water temperature in slow-moving shallow water sources can change rapidly and is strongly impacted by air temperature (Anthony et al., 2009), radiant heat, the temperatures of river and groundwater inputs, and heat transfer at the water's surface (Yu et al., 2021). In coastal Virginia, higher temperatures are of concern, as they could push species beyond tolerance thresholds, increase the competitive advantage of potential invasive species, and allow for more southerly species to invade (*VCR/LTER Proposal 2018*, 2018). Model predictions show that seagrass meadows at the VCR can be threatened by longer summer periods of warmer temperatures (Carr et al., 2012). Additionally, prolonged increases in temperature can trigger algae blooms

(Trombetta et al., 2019), increase the chance of hypoxia events, and impact the phenology in coastal organisms (Anthony et al., 2009).

Dissolved oxygen (DO) levels are directly linked to temperature, with higher temperatures having lower oxygen saturation levels and vice versa (Anthony et al., 2009). In coastal Virginia, changes in storms and precipitation can influence the amount of freshwater and nutrients as well as increasing turbidity, which can in turn lower DO (*VCR/LTER Proposal 2018, 2018*). It can also be lowered by excess organic matter decomposition stimulated by anthropogenic nutrient and organic matter runoff (Perna et al., 2005), droughts creating longer periods of low flow which increases the relative amount of pollutants (Muholland et al., 1997), and a more intense (higher) spring runoff which changes the density gradient and limits atmospheric oxygen diffusion (Kennedy et al., 1990). This decrease in DO can stress aerobic organisms, specifically benthic communities, and this issue can be made worse in lagoons with low flushing rate (Anthony et al., 2009).

With rising sea level, salt water can intrude further into lagoons, increasing salinity (Kennedy et al., 1990). In coastal Virginia, sea-level rise is a main climatic driver of state change, with the shallow slope of coastal barrier landscapes making them particularly vulnerable to both this rise and storm events (*VCR/LTER Proposal 2018, 2018*). The current rate of relative sea level rise in this area is about 4 mm/yr and is one of the highest on the Atlantic Coast (Safak et al., 2018). Periods of higher salinities that are followed by high precipitation that rapidly decreases salinity can cause species die offs as many species may not be able to tolerate this extreme changes in a short period of time paired with the influx of nutrients and sediments (Havens, 2018).

Chlorophyll-a (Chl) concentrations depend on all of the above-mentioned variables, especially temperature, which in coastal Virginia is increasing (*VCR/LTER Proposal 2018*, 2018). High Chl concentrations indicate algal blooms and increase when there is weaker water exchange (Kuang et al., 2020) and a discharge of excess nutrients into the water source (Boyer et al., 2009) from sources such as fertilizers, septic systems, sewage treatment plants and urban runoff (EPA, n.d.). Eutrophication can kill off seagrasses and other slower growing benthic macroalgae, replacing it with faster growing and higher oxygen demand macroalgae in the water column that thrive in larger nutrient load environments (Perez-Ruzfana et al., 2019). These algal blooms reduce light penetration in the water column, and lower the productivity of seagrasses and benthic organisms, further worsening nutrient loads, and causing a positive feedback loop of more water column phytoplankton growth (Boyer et al., 2009). This cycle can lead to hypoxia events, nutrient imbalances, and changes in species patterns and community structures (Perez-Ruzfana et al., 2019).

Apparent Oxygen Utilization (AOU) is the difference between equilibrium saturation concentration of water at a temperature and salinity and the observed dissolved oxygen value at that time (Biological & Chemical Oceanography Data Management Office, n.d.). In coastal Virginia, this derived value will be impacted by sea level rise, storm events, and higher temperatures (*VCR/LTER Proposal 2018*, 2018). The difference between these values arises due to factors such as atmospheric gas exchange, ventilation of carbon export (Emerson et al., 2004), and biological activities (Biological & Chemical Oceanography Data Management Office, n.d.). A negative AOU indicates that supersaturation is occurring, likely due to algal photosynthesis and higher productivity, while positive AOU's indicate high respiration and consumption (Yuan et

al., 2011). As coastal lagoons are highly productive systems and support a high number of organisms, AOU can quantify this net community metabolism.

## 2.2 High Frequency vs Low Frequency Water Quality Monitoring

High frequency monitoring provides close to real time data, allowing for very high temporal resolution. This can allow for accurate forecasting models, compliance monitoring, baseline characterization, and event based impacts (Coraggio et al., 2022). It can also allow for sub-seasonal variation to be observed, and limit the bias of fair weather sampling, and diurnal and non-storm dependent changes (Granger et al., 2018). This data can help provide more accurate information on factors such as streamflow, which can have widely varying discharges on a monthly, weekly, and daily scale (Dalley, 1986). Additionally, hotspots of poor water quality due to short term impacts such as boat traffic can be monitored using such frequent observations (Briciu-Burghina et al., 2014). These measurements can help improve environmental models, with one study finding that tides, solar irradiation, water temperature, and offshore wind speeds are the most important variables in their model (Searcy & Boehm, 2021). Using models such as the Extended Kalman Filter, DO, water temperature, and salinity can be linked to meteorological forcings and lower frequency variables such as nutrients (Pastres et al., 2003). However, there can be issues in more noise and bias in the data that can arise from environmental and instrument variables (Granger et al., 2018). These high amounts of data can also cause issues in storing, processing, and costs (Coraggio et al., 2022), as well as geographic limits in where stations will have enough power to sample.

Low frequency sampling, while having lower temporal resolution, is more cost-effective and less prone to sensor malfunctions. Pairing that with long term data sampling, over many years, it allows for clearer pictures of water quality patterns over time. Long term low frequency

data are obviously necessary in examining long-term changes, and allow more context than shorter term data (Burt et al., 2011). Low frequency observations are especially helpful for when the intended outcome is to characterize seasonal variation and trends in water quality over a long period of time (Coraggio et al., 2022) For data that vary on a longer term scale, accurate estimates can still be made (Burt et al., 2011). Long term water quality data is essential to revealing patterns in complex systems with slow emerging signals (Burt et al., 2014). These longer datasets can indicate larger scale regional hotspots in poorer water quality and link those to specific anthropogenic influences and climate change impacts (Bugica et al., 2020). This can indicate specific areas of concern to be targeted in mitigation efforts. However, the issues with lower frequency sampling can restrict our knowledge of hydrological variability and only partial understanding of a system (Burt et al., 2014). Additionally, in smaller study areas, low frequency may not be appropriate due to discharges and atmospheric events causing more sudden changes (Coraggio et al., 2022).

### 2.3 Relationship between storm events and water quality

Storm events impact water quality variables. In general, storms induced a decrease in temperatures in streams during the event (Brown & Hannah, 2007). Predictably, water quality changes after a large storm event, such as lower salinities, decreasing water clarity and increasing turbidity (Davis, et al., 2004). Diurnal variability signals for temperature and DO are overwritten during storm events (Saraceno et al., 2009). During high discharge events, such as storm events, DO and Chlorophyll-a values tend to decrease due to higher suspended sediments (Bukaveckas et al., 2020). For chlorophyll-a, there is a large variation during storm events, with the direction depending on hydrological factors and flow regimes, but an increase after storms due to higher water temperatures can be seen (Liao, 2021). Storm events predictably wash out

floating photosynthetic organisms, decreasing productivity (increasing AOU) and increasing DO during storms due to mixing (Liu et al., 2020).

Winds can induce currents, waves, and turbidity in bodies of water, which can re-aerate water and increase DO concentrations (Elbaradei & Alsadeq, 2019). Water levels change diurnally to semi-diurnally due to changing tides phases, and can be impacted by storm events. Storm surges are an abnormal rise in sea level during a storm, over that of the normal predicted level due to the astronomical tide (NOAA, 2023). They can bring in high salinity water, decrease DO concentrations, and can increase sedimentation and nutrient loading (*Aquatic*, n.d.). Air pressure can impact the dissolving of oxygen into water, with more being able to dissolve in higher air pressure (Fondriest Staff, 2010). Low pressure also allows for sea levels to rise and rapid evaporation, driving wind and storms (New Jersey Sea Grant, n.d.). Precipitation can cause increases in nutrient loading, and cause potential algal blooms and anoxic zones (National Science Foundation, 2017). It decreases both salinity because of increased freshwater input and water clarity because of turbulent waters (Swartwood, 2022).

### **3. Research Questions**

Using harmonic analysis to investigate seasonal patterns, I focused on the following questions

- 1) Are there differences between harmonic elements of high and low frequency data sites over site types, inland or ocean facing, and do these differences remain consistent during subsampling of the same frequencies?
  - 1a. How many years of simulated quarterly sampling are needed until the average variability in error plateaus?

- 2) Are seasonal components and/or storm events linked to large magnitude anomalies in water quality variables and does the direction (positive or negative) of these have consistent significant relationships with weather factors across sites?
  - 2a. Do these significant correlations indicate changing weather patterns due to climate change will significantly impact water quality?

## **4. Methods**

### **4.1 Site and Data Descriptions**

The sites of interest in this project are on the ocean side of the Eastern Shore of Virginia. The Virginia Institute of Marine Science (VIMS) at the Eastern Shore Laboratory (ESL) has high frequency YSI EXO2 Sonde land-based pumps at sites at Wachapreague (W) and Willis Wharf (WW) (Ross & Snyder, 2020). Water quality data has been provided by the College of William and Mary's Virginia Institute of Marine Science Eastern Shore Laboratory (VIMS ESL) with the assistance of ESL's Darian Kelley. Site W is located on a channel creek that occurs near sites of extensive aquaculture, and is described as having offshore weather impacts, deep channels, and tidal currents, and site WW is also located in a creek near commercial hatcheries (Ross & Snyder, 2020). For site W, the data start 3/25/2016 and end 12/31/2022 and for site WW, the data starts 10/12/18 and ends 12/24/2022 (Ross & Snyder, 2023). However, there are also large gaps in the measurements for both sites (Ross & Snyder, 2023). At both sites, these water quality measurements were taken at 15 minute intervals, with the raw data averaged to one measurement per day for seasonal and hourly for diurnal harmonic analysis. Hourly water levels were recorded at a National Oceanic and Atmospheric Administration (NOAA) site at site W (Station ID: 8631044) (NOAA Tides & Currents, 2022). Weather data for wind speed and direction, and air

pressure was recorded from the same site at 6 minute intervals (National Data Buoy Center, 2022), and was then averaged to hourly intervals for the purpose of data analysis. Precipitation data for hourly intervals were collected from National Aeronautics and Space Administration (NASA) Prediction of Worldwide Energy Resources (2022) using the site's latitude and longitude. Tidal lag and weather differences between sites were determined insignificant, and were used for both site W and WW.

The second set of water quality sampling sites are low frequency as part of the Virginia Coast Reserve (VCR) which houses lagoons as well as barrier islands (*VCR/LTER Proposal 2018*, 2018). Data (doi: knb-lter-vcr.247.17) were retrieved from the VCR website. Data was manually collected using a YSI Datasonde lowered from a small boat or from the shore at each site; chlorophyll was calculated from collected discrete water samples extracted using an acetone, methanol and deionized water solution and quantified with a spectrophotometer (McGlathery et al., 2022). Tidal cycles were recorded during time of measurement, but due to the sampling strategy, all data points were recorded during falling tides and are biased to good weather and safe boating conditions (McGlathery et al., 2022). Water residence times were estimated using a three-dimensional finite-volume coastal ocean model (FVCOM) and then validated with field observations (Safak et al., 2018). Values were estimated from the closest coordinate to each water quality site using high tide and no wind conditions, the most similar conditions to those of sampling (Safak et al., 2018).

Table 1 shows the location and dates measured of the VIMS and VCR Sites.

Table 1. Names, Coordinates and Dates Measured of Each Site

Site	Location	Latitude (Degree)	Longitude (Degree)	Dates Measured
<b>W (Wachapreague)</b>	Channel Creek	37.60772	-75.68581	3/25/16 to 12/31/22
<b>WW (Willis Wharf)</b>	Tributary Creek	37.51228	-75.80622	10/12/18 to 12/24/22
Ramshorn Channel Creek (RCC)	Mainland Creek	37.302883	-75.904642	8/26/04 to 10/11/22
Redbank Creek Mouth (RBCM)	Mainland Creek	37.460083	-75.816	8/26/04 to 10/10/22
Cattleshed Creek Mouth (CCM)	Barrier Creek	37.44292143	-75.68927765	7/28/92 to 10/10/22
Little Cobb Island (LCI)	Back-Barrier	37.305273	-75.792273	8/26/04 to 10/11/22
Machipongo Inlet (MI)	Ocean Inlet	37.36764	-75.73592	7/31/97 to 10/10/22
New Marsh (NM)	Lagoon Shoal	37.290609	-75.856815	8/26/04 to 10/11/22
Oyster Harbor (OH)	Harbor	37.28919	-75.92427	7/28/92 to 10/11/22
Phillips Creek Mouth (PCM)	Mainland Creek	37.44484653	-75.83420277	7/28/92 to 10/10/22
Quinby Inlet (QI)	Ocean Inlet	37.46709235	-75.66833496	8/25/92 to 10/10/22
Red Banks (RB)	Lagoon Shoal	37.46406076	-75.80665112	7/28/92 to 10/10/22
South Hog (SH)	Barrier Creek	37.38199	-75.71811	7/31/97 to 10/10/22
Shoal Site (SHS)	Lagoon Shoal	37.417028	-75.761194	8/26/04 to 10/10/22
Sand Shoal Inlet (SS)	Ocean Inlet	37.29038	-75.784927	8/26/04 to 10/11/22

Bolded sites indicate VIMS sites, while non-bolded are in the VCR.

### VCR and VIMS Sites



**Figure 1.** Spatial map created in ArcGIS using Imagery (WGS84) basemap showing the locations of the VIMS sites as purple dots, and the VCR sites as pink dots.

## 4.2 Data Analysis

### 4.2.1 Harmonic Analysis of Seasonal Cycles

For this project the data analysis was done in Matlab and R, unless otherwise specified, using the aforementioned data sets.

Chavuent's Criterion was used for outlier removal on the raw data in raw and hourly averaged forms. Chlorophyll-a was normalized by first adding 1 to all values to account for values of 0 ug/L, and then the common logarithm ( $\log_{10}$ ) was taken.

Data for each site were compiled into climatological day of year graphs, and a model estimate,  $y^m(t)$ , was constructed using 1<sup>st</sup> and 2<sup>nd</sup> harmonics (sine curves) fit using the formula (Wilks, 2011):

$$y^m(t) = \bar{y} + \sum_k^2 \left( a_k \cos\left[\frac{2\pi kt}{n}\right] + b_k \sin\left[\frac{2\pi kt}{n}\right] \right) \quad (1)$$

where  $k$  is the respective harmonic,  $\bar{y}$  is the mean of the  $y$  values (water quality variables),  $a_k$  is the cosine coefficient of the  $k$ th harmonic,  $t$  is day of year format,  $n$  is time period (365 days), and  $b_k$  is the sine coefficient of the  $k$ th harmonic.  $\bar{y}$ ,  $a_k$  and  $b_k$  were found using a least squares method in Matlab for each respective harmonic. Confidence intervals for the computed model parameters were calculated.

The amplitudes were found using

$$A_k = \sqrt{(a_k)^2 + (b_k)^2} \quad (2)$$

Phase shifts were found using

$$\phi_k = \arctan\left(\frac{b_k}{a_k}\right) \quad a_k > 0 \quad (3)$$

$$\phi_k = \arctan\left(\frac{b_k}{a_k}\right) + \pi \quad a_k < 0 \quad (4)$$

Date of the maximum values were found

$$t_k = \frac{n}{2\pi} \phi_k \quad (5)$$

Variances were found (Burroughs, 2003).

$$\sigma_k^2 = \frac{A_k^2}{2} \quad (6)$$

With the total variance ( $\sigma^2$ ) being the sum of the first and second harmonic variances.

Percent variance for harmonic  $k$  is:

$$pV_k = \frac{\sigma_k^2}{\sigma^2} \quad (7)$$

The reduced chi squared value was found (Glover et al., 2012)

$$\chi_v^2 = \frac{1}{v} \sum_{i=1}^N \frac{(\hat{y}_i - y_i)^2}{\sigma_i^2} \quad (8)$$

Where

$$v = N - m \quad (9)$$

With  $N$  being the number of observations,  $m$  is the number of calculated variables,  $\hat{y}_i$  is the model fit estimate,  $y_i$  is the observed value, and  $\sigma_i^2$  is the variance of the observed data.

The local minimum ( $t_{min}$ ) and maximums ( $t_{max}$ ) of the composite harmonics were computed using the zero-points of the first derivative with respect to time,  $t$ , using Equation 1.

The amplitude of the composite harmonics was found from:

$$A_{max} = \frac{t_{max} - t_{min}}{2} \quad (10)$$

Confidence intervals were calculated for the harmonic elements by subsampling and bootstrapping between the previously calculated model parameters confidence intervals 200 times.

Using the Matlab Code by Mertens (1996), oxygen saturation was calculated by

$$O_{sat} = \exp(c_1 + \frac{c_2}{t} + c_3 \log(te) + c_4 t + s(d_1 + (d_2 + d_3 t)t) \quad (11)$$

Where  $c_1$  is -173.4292,  $c_2$  is 249.6339,  $c_3$  is 143.3483,  $c_4$  is -21.8492,  $d_1$  is -0.033096,  $d_2$  is 0.014259,  $d_3$  is -0.0017, with  $s$  (salinity (ppt)) and  $te$  (temperature ( $^{\circ}C$ )) being the inputted values. This yielded values in mL/L, which is converted to mg/L by dividing by 0.7000.

AOU was calculated by

$$AOU = O_{sat} - DO \quad (12)$$

Where DO is the measured value (mg/L) at the time of the respective  $O_{sat}$ .

Random subsampling was performed on the composite harmonic formula at the same frequency of the VCR inland sites for each parameter at the VIMS sites (202 temperature, 190 salinity, 175 DO, 164  $\log_{10}(\text{Chl})$ , 164 AOU values selected for each trial) 200 times. For each trial, a composite harmonic was fit using Equation 1. Averages, standard deviations, standard error, and confidence intervals were calculated for each parameter in the formula and harmonic element.

$$\text{Percent Difference} = \frac{|V_1 - V_2|}{\left[\frac{(V_1 + V_2)}{2}\right]} \times 100 \quad (13)$$

Where  $V_1$  is complete data harmonic element and  $V_2$  is the average subsampled value.

Percent differences were calculated using Equation 13, between the complete and averaged subsampled values for each parameter at W and WW.

Spatial maps of the sites were made in ArcGIS using the calculated dates and values of the composite harmonic maximums (temperature, salinity, and  $\log_{10}(\text{Chl})$ ), AOU) or minimums (DO), as well as the seasonal amplitudes.

#### 4.2.2. Generalized Least Squares analysis of synoptic anomalies

$$\text{Parameter Anomalies} = y_i - \hat{y}_i \quad (14)$$

Generalized Least Squares (GLS) allows for linear fits to be created when assumptions of linear regression are violated, such as absence of serial correlation (temporal autocorrelation) (Taboga, 2021). Points that are closer together are more similar than points that are farther apart, and a correlation structure must be used to account for this to see accurate relationships. GLS was performed on parameter anomalies over time calculated using Equation 14 in order to see if there were any long term changes for each of the sites and variables.

#### 4.2.3 Simulated Quarterly Sampling

The respective daily averaged values for sites W and WW were sorted into seasons (winter (December, January, February), spring (March, April, May), summer (June, July, August), and fall (September, October, November)). Picking the season with the most values to represent the maximum years of quarterly sampling ( $m_y$ ), values are randomly subsampled  $2:m_y$  times per season and harmonic analysis is performed 200 times, and an average was taken of each harmonic formula element to compute a fit for each year.

$$\text{Average Error} = \text{Mean}(|\text{Full Model Point} - \text{Subsampled Model Point}|) \quad (15)$$

Using equation 15, the average error (in terms of uncertainty in model variables due to sampling frequency) for each data point 1:365 is taken for each successive year, and is plotted against its respective year, creating a decaying curve scatter plot.

$$\text{Relative Change} = \frac{|X_2 - X_1|}{X_1} \times 100 \quad (16)$$

Where  $X_1$  is the fitted value point previous value and  $X_2$  is the current fitted value point.

A logarithmic regression model was fit on the average error vs years of sampling scatter plot using R. This method was chosen as it allows for decay to be consistent in direction (downwards) to make meaningful calculations of relative change, as the raw values show some natural variability in direction as time goes on. Relative change was calculated using Equation 16

between each year's fitted value of average error generated from the logarithmic model. Relative change values were then standardized using the mean and standard deviation of all of the relative change values in order to compare across variables. Thresholds of 1%, 0.5%, and 0.25% standardized relative change were chosen as they indicate plateauing of relative change between years. While standardized variables are unitless, the percentage (%) unit is used to guide audiences in what the variable represents.

The same steps were performed using the average percent difference across harmonic elements (date and value of minimum/maximum and seasonal amplitudes) between the subsampled and full model calculated using Equation 13 to validate the results.

#### *4.2.4 Diurnal Anomalies*

For diel cycles at sites W and WW, parameter data was converted to hourly averages, and for each week of the year was converted to an hour of day format in order to run harmonic analysis as done above, using  $n=24$  instead of 365 in Equation 1. Variables were grouped by week of year to minimize anomalies due to changes throughout months that may be very different at the beginning versus the end, such as in spring, to focus on high magnitude anomalies that were solely deviations from the normal cycle. Anomalies were computed using differences from the model fit in Equation 14. A positive anomaly represents a value that is higher than expected while a negative anomaly represents a value that is lower than expected. The top and bottom 5% of these anomalies were calculated, and then separated into negative and positive groupings, and then sorted seasonally, into winter (December, January, February), spring (March, April, May), summer (June, July, August), and fall (September, October, November).

$$\text{Water Level Anomalies} = W_{exp} - W_{obs} \quad (17)$$

Where  $W_{exp}$  is the expected hourly water level value predicted by NOAA, and  $W_{obs}$  is the hourly observed value.

Using R, a GLS with a correlation term to account for temporal autocorrelation was performed to test for significant relations to weather factors (wind speed (m/s), water level anomalies (m) (calculated using Equation 17), air pressure (mb), and precipitation (mm/hr)) for each season and direction (positive or negative) of anomalies.

For the diurnal anomalies relation to storm events, these events were classified using the NOAA Storm Events Database, which identified the date and type of event in sites W and WW using their county and verified by signals seen in the weather data at the sites. Only storms over 12 hours were investigated in order for long enough time periods and changes to be seen. Heavy rain is categorized as a large amount of rain that does not cause a flash flood, but does cause damage (National Weather Service. 2021). Tropical storms are categorized as a tropical cyclone in which the 1-minute sustained surface wind ranges from 39 to 73 mph (17 to 33 m/s) (National Weather Service, 2021). Winter weather is categorized as a winter precipitation event that causes death, injury, or significant impact to commerce/travel, while a winter storm is categorized as a winter weather that has more than one significant hazard (ex: heavy snow, ice, etc.), and are grouped together due to their similarities (National Weather Service, 2021). A coastal flood is defined as flooding due to strong, persistent onshore winds, high astronomical tide, and/or low atmospheric pressure resulting in damage or injuries (National Weather Service, 2021). Hurricanes were identified using the NOAA Historical Hurricane tracks website, and selected using latitude and longitude of respective sites, and subsequent weather events due to these tracks were noted. A hurricane is categorized as a tropical cyclone in which the maximum 1-minute sustained surface wind is 74 mph (33 m/s) or greater (National Weather Service. 2021).

**Table 2. Classification of Weather Events**

Storm Event	Discrete # of Events (W)	Discrete # of Events (WW)
Tropical Storm	2	1
Heavy Rain	7	4
Winter Storm/Winter Weather	4	2
Coastal Flood	4	2
Hurricane	1	3

Time series data was categorized as before event, during event, and after event, all the same length as the event itself. Analysis was done in R, using a GLS model with a correlation term, in order to account for temporal autocorrelation to test for significant relationships between weather factors and water quality parameter anomalies before, during, and after that event.

## 5. Results and Discussion

### 5.1 High vs Low Frequency Seasonal Harmonic Analysis

#### 5.1.1 Temperature

For all sites, the first harmonic cycle dominates, indicating an annual cycle (Table A1, Figure 2). Annual temperature changes are primarily driven by meteorological factors and physical hydrological characteristics (Benyahya et al., 2007). The harmonic curves strongly show that the warmest temperatures are in summer and coolest in the winter, highlighting the impact of seasonal air temperature and solar radiation changes (Figure 2).

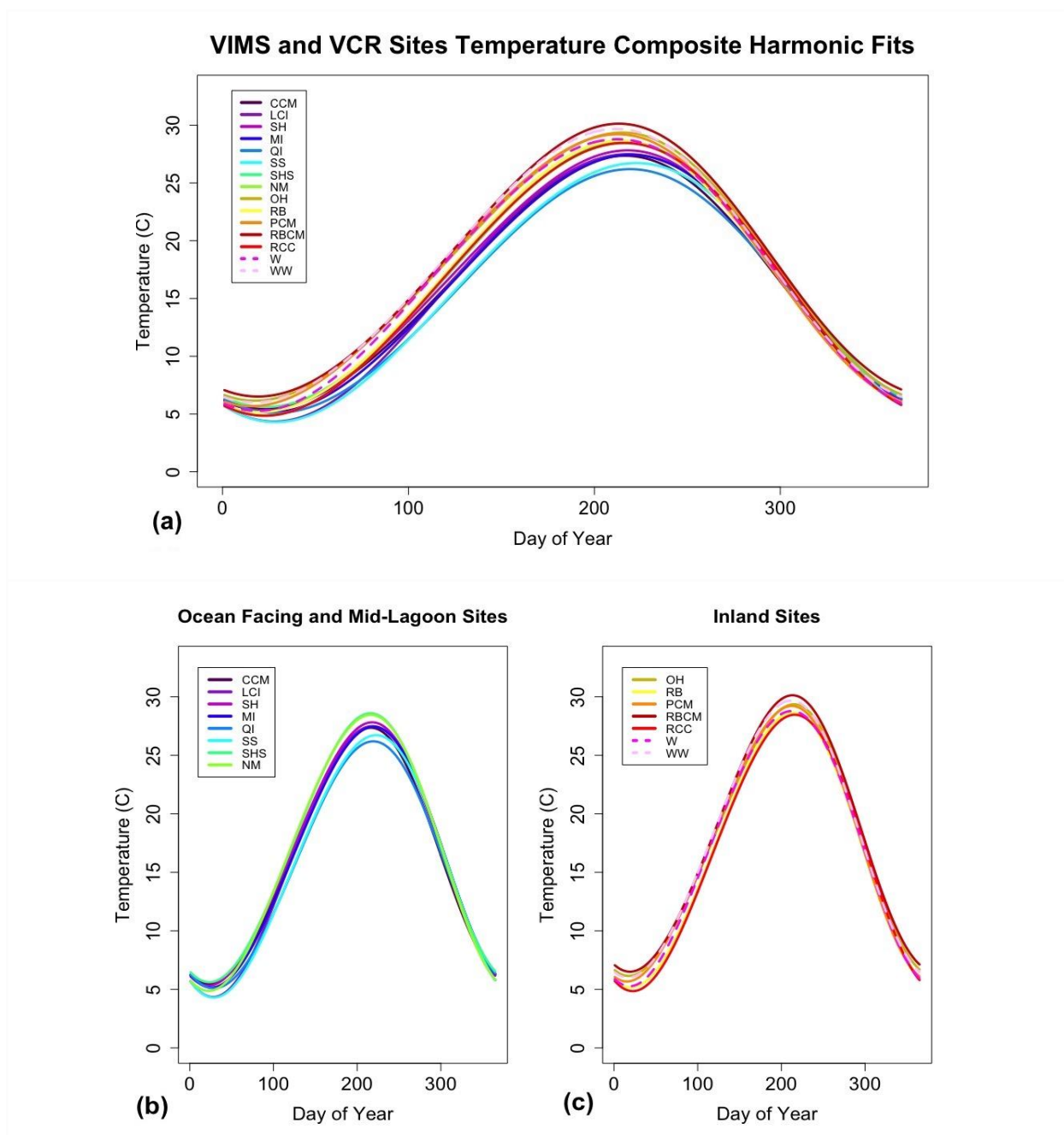
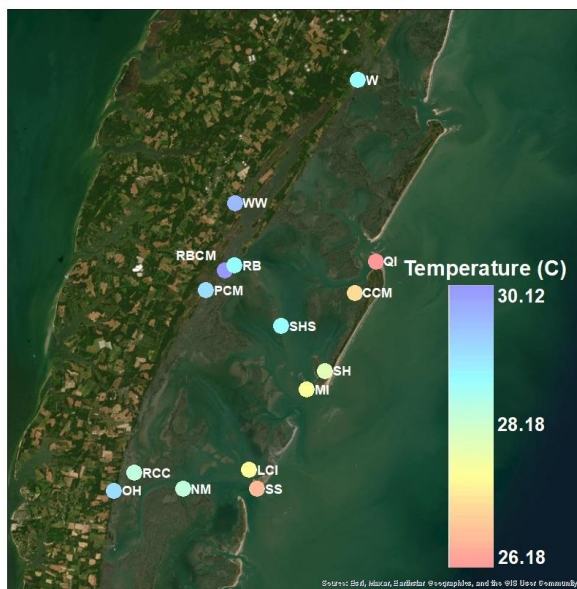


**Figure 2.** Temperature Composite Harmonic Fits. **(a)** All VIMS (W and WW) and VCR sites (CCM, LCI, SH, MI, QI, SS, SHS, NM, OH, RB, PCM, RBCM, and RCC). **(b)** Ocean facing and mid-lagoon sites. **(c)** Inland sites.

Inland sites generally have slightly earlier dates for summer peak temperatures (average of  $213.6 \pm 1.566$  days), and higher maximum peak values (average of  $29.21 \pm 0.6093$  °C) and seasonal amplitudes (average of  $11.77 \pm 0.08151$  °C) compared to ocean facing sites (average of  $218.3 \pm 2.405$  days,  $27.51 \pm 0.6649$  °C, and  $11.26 \pm 0.2987$  °C) (Figures 2 and 3, Table A1).

Inland sites are more impacted by freshwater inputs with shallower depths that allow for more rapid and intense temperature changes, while ocean facing sites are routinely exposed to cooler ocean water limiting large temperature variations, paired with their much lower residence times (Safak et al., 2018, Figure 3). Site QI had both a lower seasonal peak temperature ( $26.18 \pm 0.05263 \text{ }^\circ\text{C}$ ) and amplitude ( $10.58 \pm 0.03692 \text{ }^\circ\text{C}$ ) that could be related this site having the longest time series of the 3 inlets, perhaps giving a more accurate temperature model or water inflow patterns being more optimal for lower maximum temperatures and amplitudes (Figure 3, Table A1).

(a) VCR and VIMS Sites Maximum Temperature Values



(b) VCR and VIMS Sites Temperature Seasonal Amplitudes

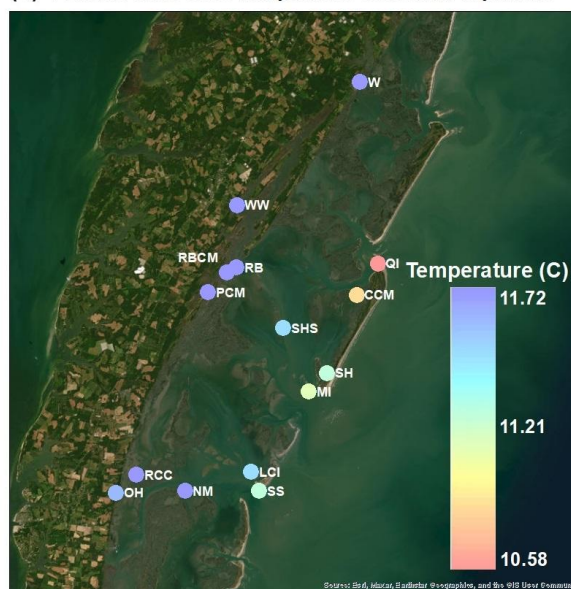
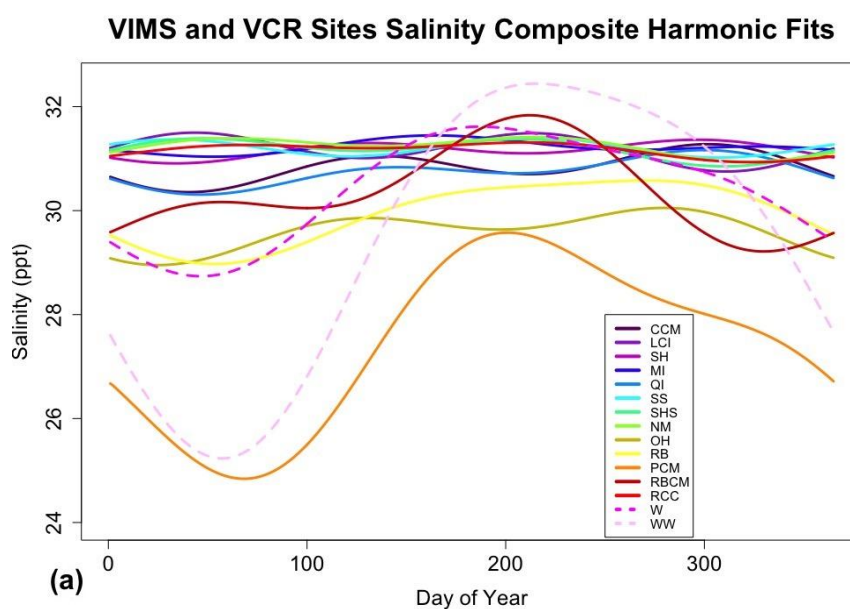


**Figure 3** Spatial maps of VCR and VIMS sites, where site codes are as in Figure 2. **(a)** Maximum temperature values. **(b)** Seasonal amplitudes.

Comparing full vs subsampled data for sites W and WW, there was a less than 0.12% average percent difference between the harmonic elements, indicating that 202 samples is enough to show almost the same harmonic results as a full high frequency dataset (Table A6).

### 5.1.2 Salinity

For salinity there was a mix of dominating harmonics at the sites, with all inland sites being dominated by the first harmonic and most ocean facing sites being dominated by the second harmonic besides sites QI and NM (Table A2, Figure 4). Salinity variations throughout the year depend on the effects of mixing, evaporation, precipitation, and atmospheric circulation (Sachithanathan, 1969). The seasonal fluctuations in freshwater input on the inland sites force a more annual cycle, while the ocean facing sites are more mitigated with the stronger impact of tidal flushing of the nearby ocean which has an overall more stable seasonal cycle due to its large size and dependence on the global water cycle (Figure 5, NASA, n.d.). Sites QI and NM having a more impactful annual cycle indicates other factors being greater than tidal flushing (Figure 5).



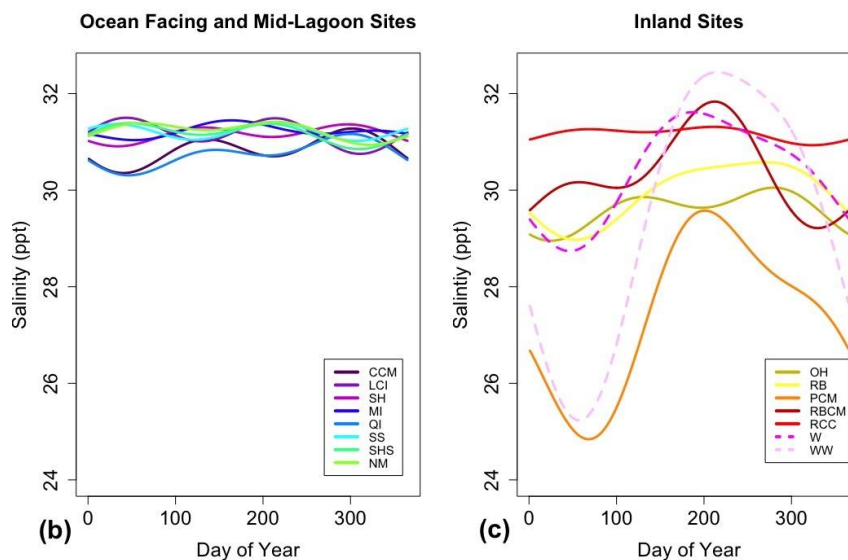


**Figure 4.** Salinity Composite Harmonic Fits. **(a)** All VIMS and VCR sites. **(b)** Ocean facing and mid lagoon sites. **(c)** Inland sites.

In general, ocean facing and mid-lagoon sites show less intra-site and temporal variability than inland sites (Figure 4). Most sites have dates of maximum values generally contained to mid to late year (inland sites average of  $227.1 \pm 26.96$  days and ocean facing and mid-lagoon sites average of  $219.0 \pm 56.44$  days), however sites SHS ( $61.55 \pm 5.755$  days) and MI ( $165.4 \pm 4.769$  days) fall earlier, possibly related to the inflow of ocean water at that inlet (Figure 4, Table A2). The inland sites have more variable maximum values (average of  $31.16 \pm 0.7618$  ppt) and higher seasonal amplitudes (average of  $1.606 \pm 0.8415$  ppt), likely due to their differences in freshwater input and/or longer residence times, while ocean facing and mid-lagoon sites have consistently higher maximum values (average of  $31.51 \pm 0.05530$  ppt) and lower amplitudes (average of  $0.4520 \pm 0.0576$  ppt), due to tidal impacts (Figure 5, Table A2).

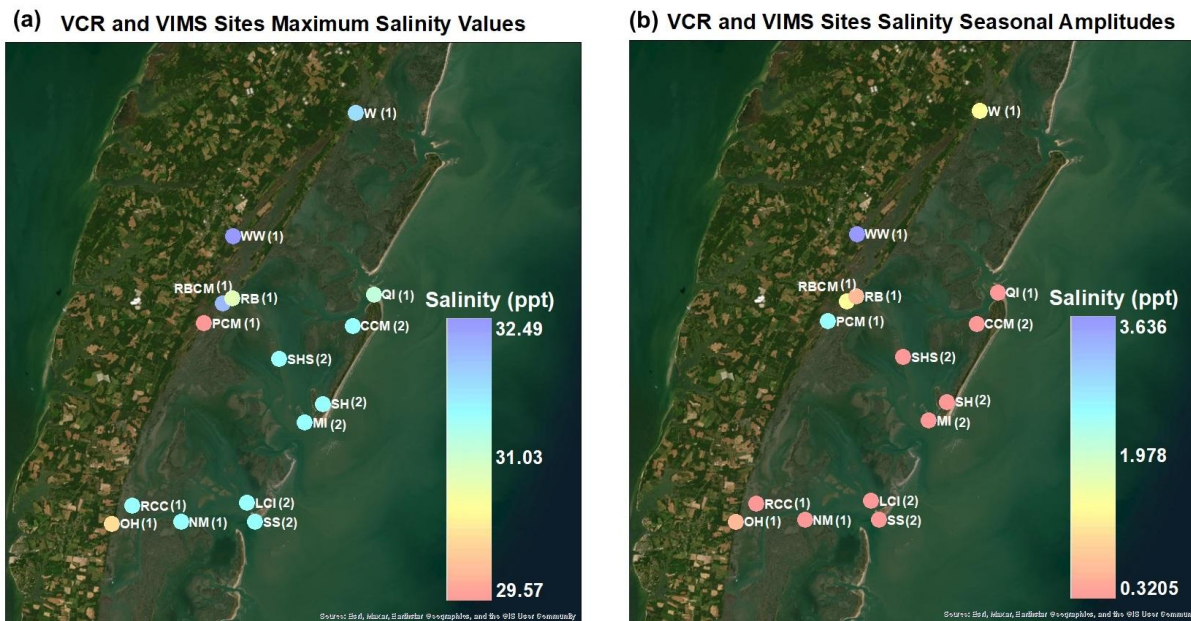


**Figure 5.** Spatial maps of VCR and VIMS sites, where (1) indicates first harmonic dominating and (2) indicates second harmonic dominating. **(a)** Maximum salinity values. **(b)** Seasonal amplitudes.

There was a larger difference between the bootstrapped and full data sets of salinity at VIMS sites W and WW. Site W had an average of 2.558% difference between the harmonic elements, with the highest being the seasonal amplitude (4.286%) (Table A6). Site WW had a lower 0.4703% average difference across its harmonic elements (Table A6). Site W having a higher percentage means more uncertainty in the bootstrapping, meaning 190 data points are not able to show as concise a picture as temperature, with harmonic models benefiting from more data availability.

### 5.1.3 DO

For DO, all sites were dominated by the first harmonic (Table A3, Figure 6). DO has an inverse relationship with temperature, where the warmer water in the summer months leads to lower concentrations of DO (Figure 6). This dip can also be accounted for by annual factors such as air temperature, as well as circulation, vertical mixing, air-sea gas exchange, photosynthetic oxygen production, and use of oxygen due to decomposition of organisms (Kim et al., 2018).

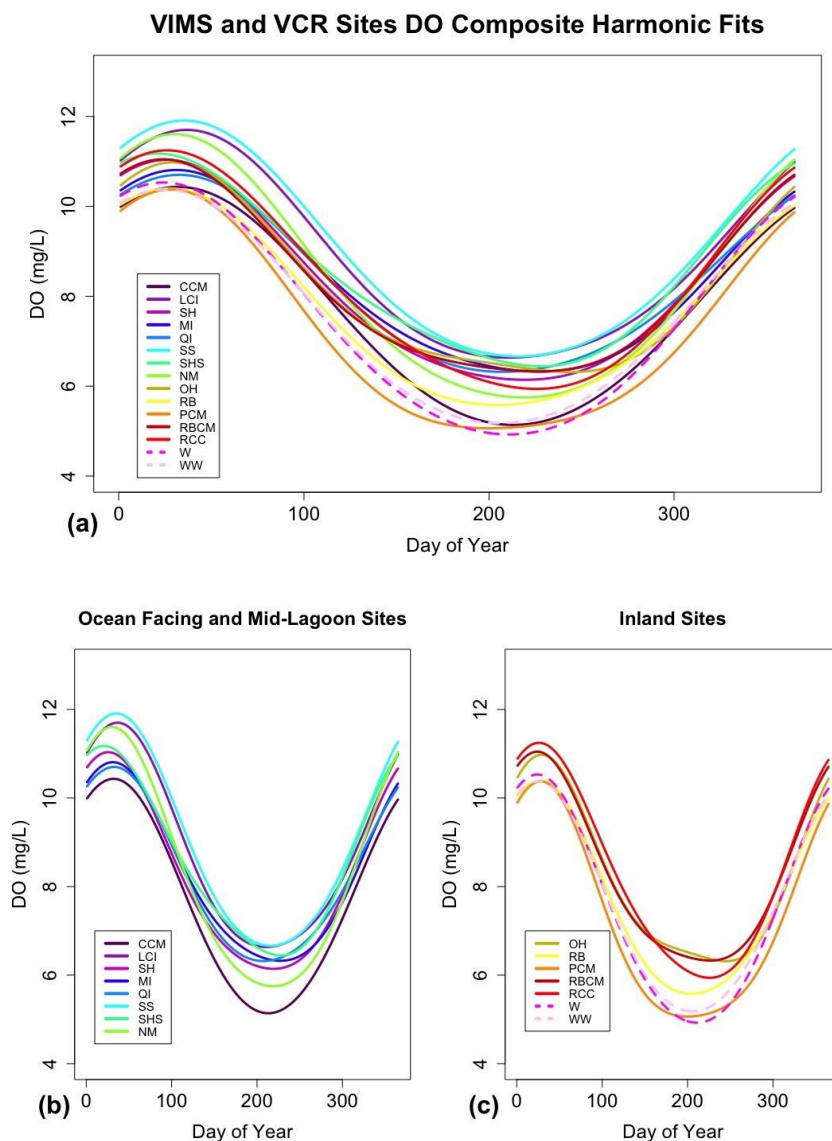


**Figure 6.** DO Composite Harmonic Fits. **(a)** All VIMS and VCR sites. **(b)** Ocean facing and mid lagoon sites. **(c)** Inland sites.

Inland sites generally have earlier to mid dates of minimum DO (average of  $216.4 \pm 8.586$  days), with the exception of site OH ( $236.9 \pm 3.439$  days) being much later, and more variable minimum DO values (average of  $5.555 \pm 0.4243$  mg/L) and seasonal amplitudes (average of  $2.564 \pm 0.1171$  mg/L) (Figures 6 and 7, Table A3). Site OH being later could be related to it having a much longer residence time, than other inland sites, with its semi enclosed shape not allowing for much flushing (Safak et al., 2018, Figure 6). The inland sites having more

variation in their harmonic elements is likely related to the range of residence times and water depths (Figure 7, Safak et al., 2018). Ocean facing and mid-lagoon sites have higher minimum values (average of  $6.093 \pm 0.3587$  mg/L), save for site CCM ( $5.108 \pm 0.04057$  mg/L), and more low to mid range seasonal amplitudes (average of  $2.559 \pm 0.1619$  mg/L), with inlet sites QI ( $2.238 \pm 0.02600$  mg/L) and MI ( $2.229 \pm 0.03301$  mg/L) being much lower and site NM ( $3.003 \pm 0.03457$  mg/L) being much higher (Figure 7, Table A3). Site NM is a lagoon shoal, and therefore experiences higher seasonal variability in both vegetation and water depth, while inlet sites QI and MI are more regulated by cooler ocean water mitigating large DO swings (Figure 7).

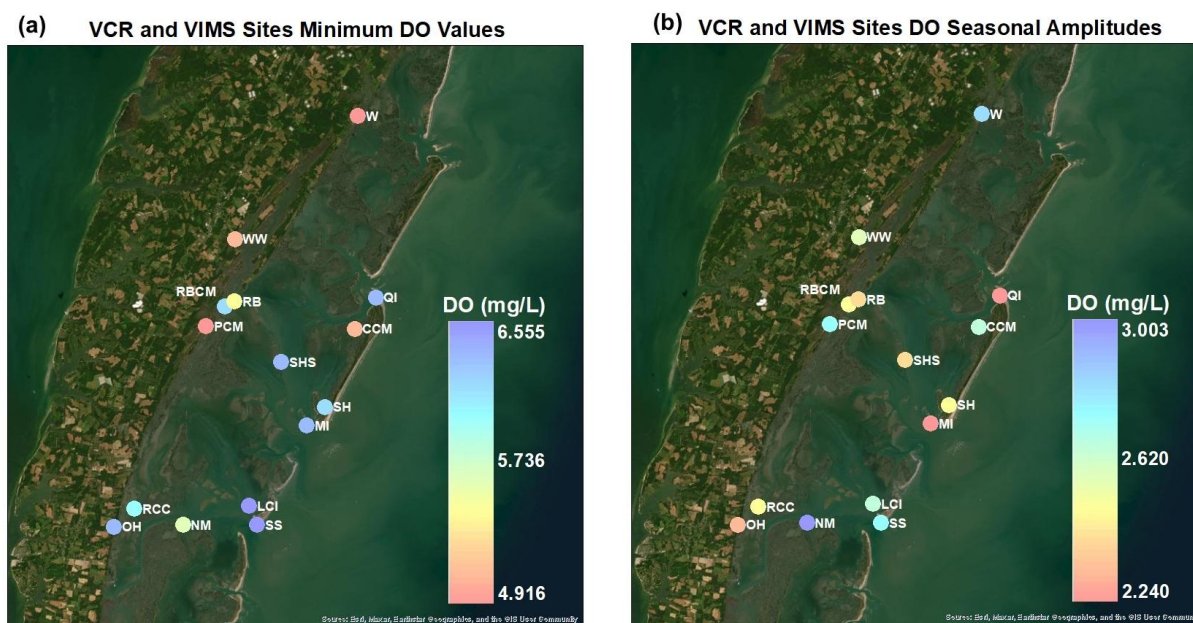
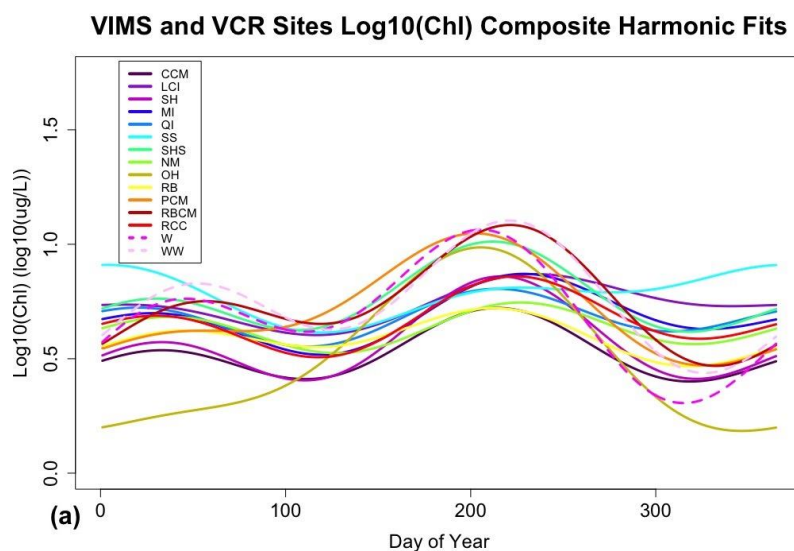


**Figure 7.** Spatial maps of VCR and VIMS sites. **(a)** Minimum DO values. **(b)** Seasonal amplitudes.

There was a smaller difference between the bootstrapped and full data sets DO with both VIMS sites W and WW having less than an average 0.22% average percent difference across their harmonic elements (Table A6). DO is inversely related to temperature, so both variables being similar in their percent differences is consistent with the harmonic models of temperature, and 175 values is enough to give an accurate harmonic model of the site.

#### 5.1.4 Chlorophyll-a

Chlorophyll-a (Chl) is a measure of phytoplankton biomass and was log transformed prior to analysis. For  $\log_{10}(\text{Chl})$ , inland sites generally had a mix of dominating harmonics, while ocean facing sites were generally 1st harmonic save for sites QI and CCM (Table A4, Figure 8). Sites QI and CCM are likely mitigated from stronger seasonal cycles due to ocean water inflow (Figure 8). Seasonal cycles of chlorophyll can be impacted by nutrient inputs, temperature, light availability (del Carmen Jiménez-Quiroz et al., 2021), as well as tide mixing, seasonal winds, upwelling, and stratification (Robles-Tamayo et al., 2020). Specifically, in lagoons, the concentrations seem to be most impacted by hydrology, meaning meteorological factors like wind, rainfall, and evaporation, and river runoff (Salas-Perez & Gonzalez-Gandara, 2016).



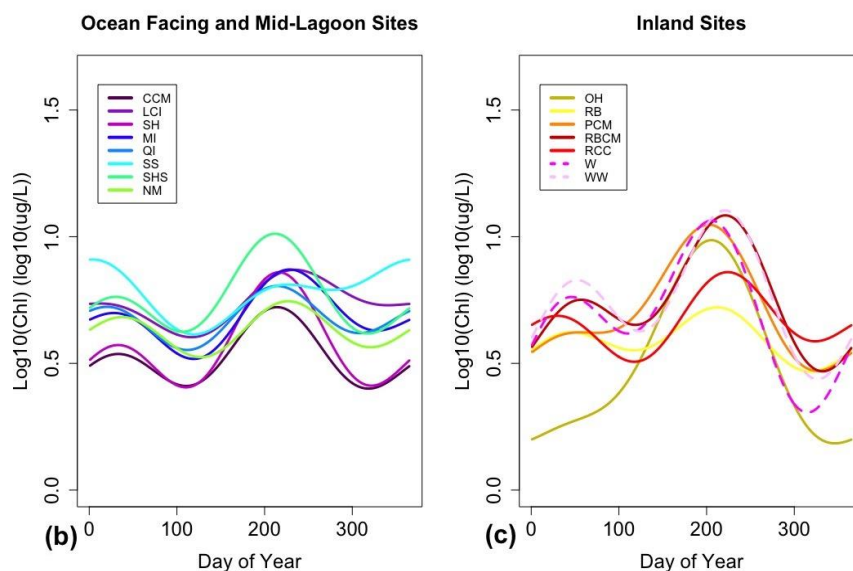


**Figure 8.**  $\text{Log}_{10}(\text{Chl})$  Composite Harmonic Fits. (a) All VIMS and VCR sites. (b) Ocean facing and mid lagoon sites. (c) Inland sites.

In general all sites had very close dates of maximum  $\text{log}_{10}(\text{Chl})$  values around mid year (inland sites having an average of  $214.8 \pm 6.516$  days and ocean facing and mid-lagoon sites having an average of  $234.6 \pm 27.06$  days), with site SS ( $323.5 \pm 4.955$  days) being much later (Figure 8, Table A4). The peak value that late in the year is very interesting and not seen at other sites and is likely related to water factors such as potentially high flushing rates during the summer that dampen the concentrations at that time (Figure 8). The inland sites have higher maximum values (average of  $8.817 \pm 0.2747$   $\mu\text{g/L}$ ) and seasonal amplitudes (average of  $1.018 \pm 0.1964$   $\mu\text{g/L}$ ), save for sites RB ( $0.3806 \pm 0.01635$   $\mu\text{g/L}$ ) and RCC ( $0.5201 \pm 0.02167$   $\mu\text{g/L}$ ) (Table A4). These sites are more likely to experience stagnant nutrient rich waters due to their longer residence times, increasing their peaks and amplitudes (Figures 8 and 9, Safak et al., 2018). Sites RB and RCC being lower than other inland sites could be due to experiencing more mixing and lower nutrient availability, dampening both the maximum values and seasonal amplitudes (Figure 9). Ocean facing and mid-lagoon sites have lower maximum values and seasonal amplitudes (averages of  $6.175 \pm 0.1658$   $\mu\text{g/L}$  and  $0.4909 \pm 0.05748$   $\mu\text{g/L}$ ) (Figure 8 and

9, Table A4). These site types being lower in both maximum value and seasonal amplitude is likely related to tidal flushing mixing the water column and cooler ocean water that is less likely to carry nutrients (Figure 9).

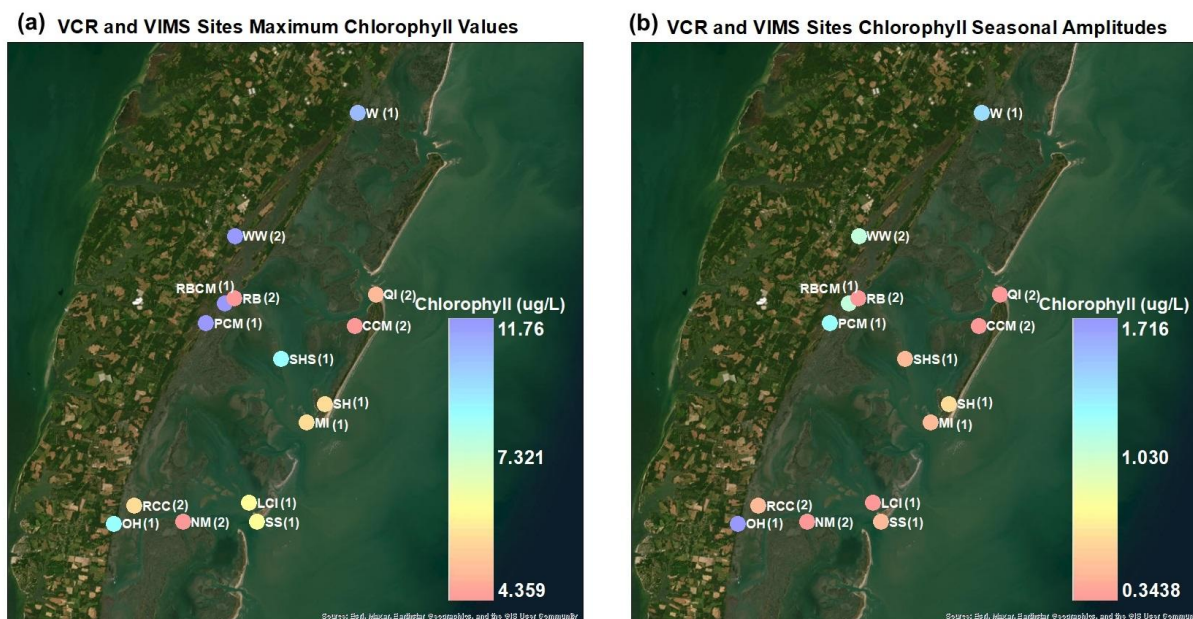


**Figure 9.** Spatial maps of VCR and VIMS sites where (1) indicates first harmonic dominating and (2) indicates second harmonic dominating. (a) Maximum Chl values. (b) Seasonal amplitudes.

There was a smaller degree of difference between the bootstrapped and full data sets of  $\log_{10}(\text{Chl})$  at the VIMS sites, with site W having an average of 0.1948% difference across elements and site WW having a higher 0.5417% average difference across its harmonic elements (Table A6). This indicates that 164 values is enough to give a pretty accurate sense of the seasonal patterns at these sites (Table A6).

### 5.1.5 AOU

For AOU, all sites were dominated by the first harmonic (Table A5, Figure 10). AOU is related to many of the same factors as DO, as well as biological activity and depth to the surface (Biological & Chemical Oceanography Data Management Office, n.d.). The solubility of oxygen is directly related to temperature, being lower in warmer air temperatures (Boyer et al., 1999),

which in turn would lead to summer months having lower oxygen solubility, as well as DO. In previous studies, higher concentrations of AOU were found in the summer and fall months, with values closer to zero in the spring and winter time (Calleja et al., 2019).

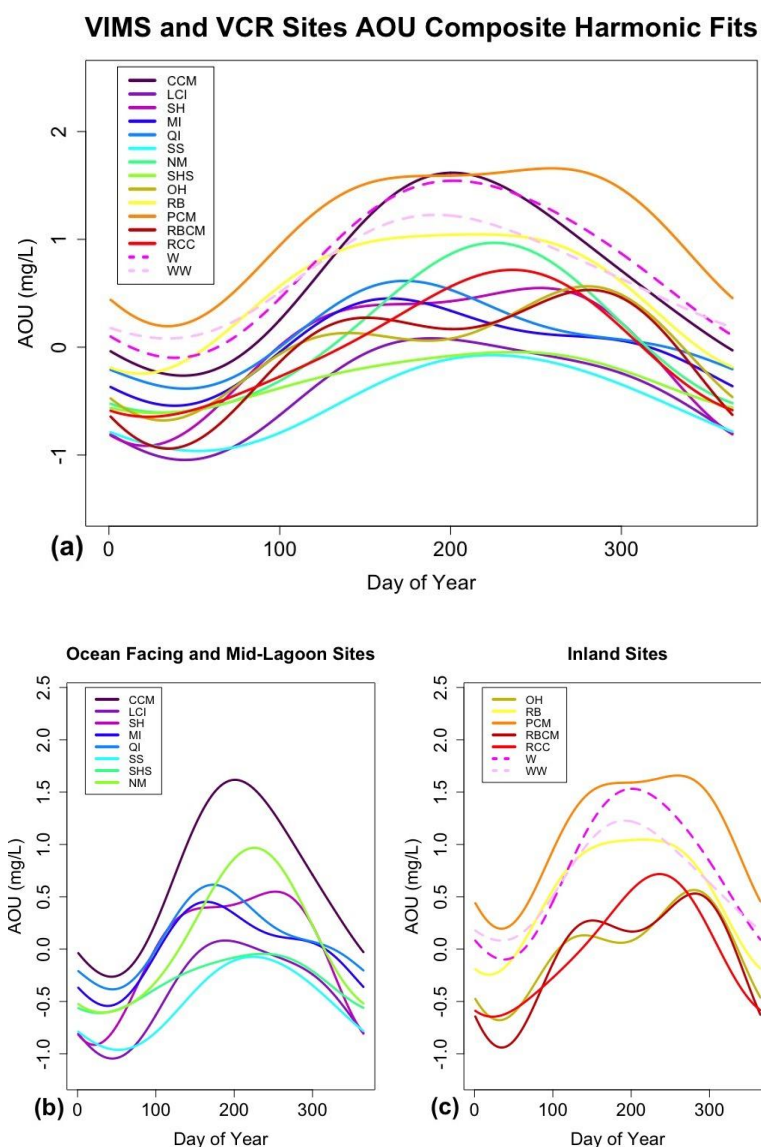


**Figure 10.** AOU Composite Harmonic Fits. **(a)** All VIMS and VCR sites. **(b)** Ocean facing and mid lagoon sites. **(c)** Inland sites.

In general, inland sites had later dates of maximum values (average of  $240.8 \pm 26.49$  days) of AOU, save for sites W ( $201.6 \pm 1.212$  days) and WW ( $194.2 \pm 3.012$  days), while ocean facing and mid-lagoon sites were more variable (average of  $211.5 \pm 19.23$  days) (Figure 10,

Table A5). The inland sites had mid to higher maximum values (average of  $1.129 \pm 0.3170$  mg/L) and seasonal amplitudes (average of  $0.7677 \pm 0.08016$  mg/L), while ocean facing and mid-lagoon sites were generally slightly lower (averages of  $0.6343 \pm 0.3952$  mg/L and  $0.7004 \pm 0.1335$  mg/L) except for site CCM ( $1.630 \pm 0.04602$  mg/L and  $0.9924 \pm 0.03533$  mg/L) (Figures 10 and 11, Table A5). Site CCM had a deviation from the general pattern of DO for ocean facing sites as well, indicating that something there is impacting productivity and/or respiration (Figure 11). Inland sites having higher maximum values indicate higher respiration and consumption, which could be related to proximity to marsh and sediment that experience higher bacterial respiration (Figure 11). Ocean facing and mid-lagoon sites are deeper and more turbulent with shorter residence times, explaining the lower AOU (Figure 11).

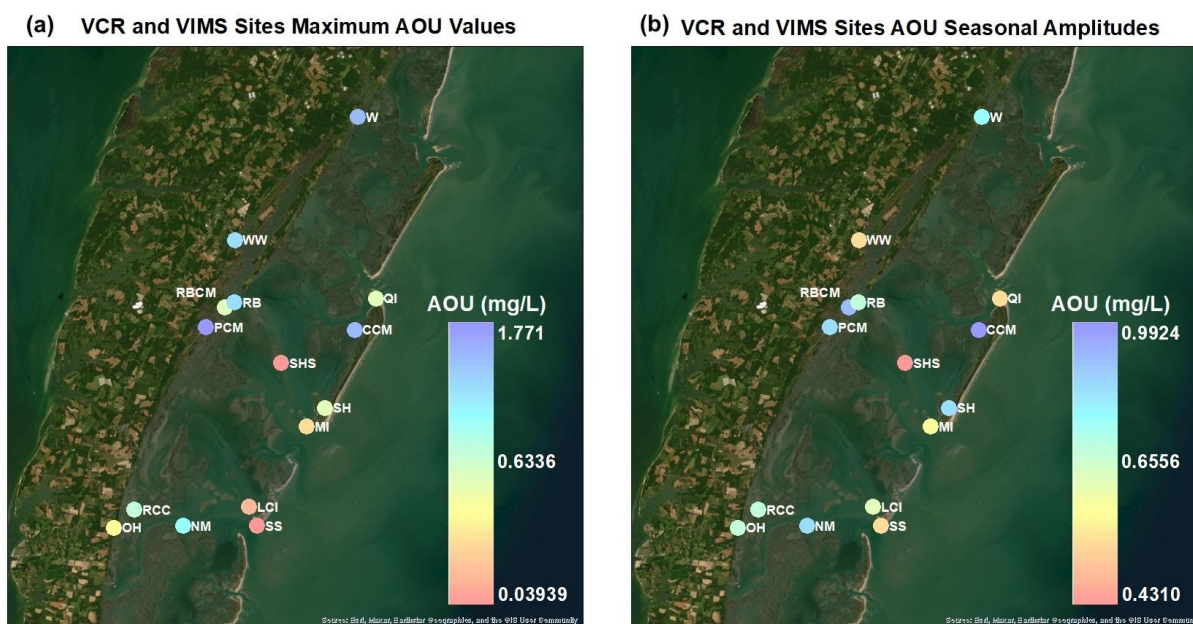


**Figure 11.** Spatial maps of VCR and VIMS sites. **(a)** Maximum AOU values. **(b)** Seasonal amplitudes.

There was a smaller degree of difference between the bootstrapped and full data sets of AOU, with VIMS site W having an average 0.3576% and site WW an average 1.149% difference (Table A6). This indicates that the 164 values give pretty accurate results in modeling AOU, more so at site W than site WW.

### 5.1.6 Long Term Changes

$\log_{10}(\text{Chl})$  had the most long term changes at 8 sites, followed by salinity at 6 sites, temperature at 3 sites, AOU at 3 sites, and DO at 0 sites (Figure 12).

At all sites except for site WW,  $\log_{10}(\text{Chl})$  increased over time, which is likely related to the length of the data set and low frequency allowing for the noise of high frequency data over a shorter period of time to be ignored (Figure 12). At the inland mid-lagoon cluster of sites, there is a co-occurrence of increasing temperature and  $\log_{10}(\text{Chl})$  values, which makes sense as warmer temperatures are ideal for algal growth (Figure 12).  $\log_{10}(\text{Chl})$  is also increasing at 2 inlet sites, QI (0.01985 ug/L/year) and MI (0.04354 ug/L/year), as well as ocean facing site SH (0.04201 ug/L/year), indicating that these changes are not just limited to inland, and that even areas with lower concentrations of  $\log_{10}(\text{Chl})$  and high rates of flushing are still being impacted (Figure 12, Table A7). Site WW (-0.1474 ug/L/year) decreasing could be related to hydrodynamic factors, as it is a creek, or the shorter time of measurement, potentially currently experiencing temporary decreases over the last few years that could change as monitoring continues (Figure 12, Table A7). Site RCC had the largest positive increase (0.5364 ug/L/year), likely related to nutrient availability there (Table A7).

Salinity was increased over time at many inland sites, and at 2 ocean facing sites, QI (0.06781 ppt/year) and CCM (0.06723 ppt/year) (Figure 12, Table A7). At the same mid lagoon cluster mentioned previously, salinity increases co-occur with temperature and  $\log_{10}(\text{Chl})$ , likely related to both saltwater intrusion and warmer water temperatures due to climate change that also fosters growth (Figure 12). The ocean facing sites increasing in salinity could be related to sea level rise increasing salinity there (Figure 12). Site W had the most noticeable and largest increase in salinity per year (0.2890 ppt/year), likely related to the shorter time series as well as

higher frequency of sampling allowing for smaller variations to be observed as well as sampling through all tidal phases (Table A7).

Temperature increases were limited to the mid lagoon inland site cluster, likely related to shallower waters being more susceptible to changing temperatures (Figure 12). Site RBCM had the largest increase in temperature per year ( $0.09140\text{ }^{\circ}\text{C}/\text{year}$ ), likely related to the co-occurring decrease in AOU, as the lower AOU indicates higher productivity which can increase in higher temperatures (Table A7).

AOU increased at just one site, indicating higher consumption rates, and decreases at 2, indicating higher productivity, likely related to higher algal rates that co-occur there (Figure 12). The positive trend in AOU at site W ( $0.04180\text{ mg/L}/\text{year}$ ) could be related to rise in salinity negatively impacting productivity and flora (Figure 12, Table A7). The largest negative trend for AOU was at site RBCM ( $-0.06560\text{ mg/L}/\text{year}$ ), which also has the highest increase in temperature, likely due to higher temperatures potentially being able to increase productivity (Table A8).



**Figure 12.** Spatial map of significant long term changes in water quality variables at VCR and VIMS sites.

### 5.1.7 Simulated Quarterly Sampling

Estimating the average errors in the estimate of the harmonic seasonal cycles between the full data set and a subsampled year, referred to as average are for the rest of this section, can be accomplished using simulated quarterly sampling. For temperature, both sites W and WW take 25-29 years to reach less than 1% standardized relative change between years and 54-62 years to reach less than 0.25% (Figure 13 and Table A8). For salinity, it takes both sites 25 years to reach 1% standardized relative change between years, and 44-54 years to reach 0.25% (Table A8). For DO, sites take 24-27 years to reach less than 1% standardized relative change between years, and 52-57 to reach 0.25% (Table A8). For  $\log_{10}(\text{Chl})$ , sites take 24-25 years to reach less than 1% standardized relative change, and 51-53 years for 0.25% (Table A8). Finally, for AOU it takes 25-26 years to reach less than 1% standardized relative change and 53-54 years to reach 0.25% (Table A8). These results are validated by performing the same methods on average percent difference of harmonic element values, the dates of reaching the thresholds only varying around 1-2 years (Table A9). The variables are very similar in reaching less than 1% standardized relative change between years, but there is more variability in reaching 0.25%, the “true” plateau (Table A8). DO and  $\text{Log}_{10}(\text{Chl})$  are the variables that reach the 1% threshold first, while salinity is the first to reach the 0.25% threshold (Table A8).

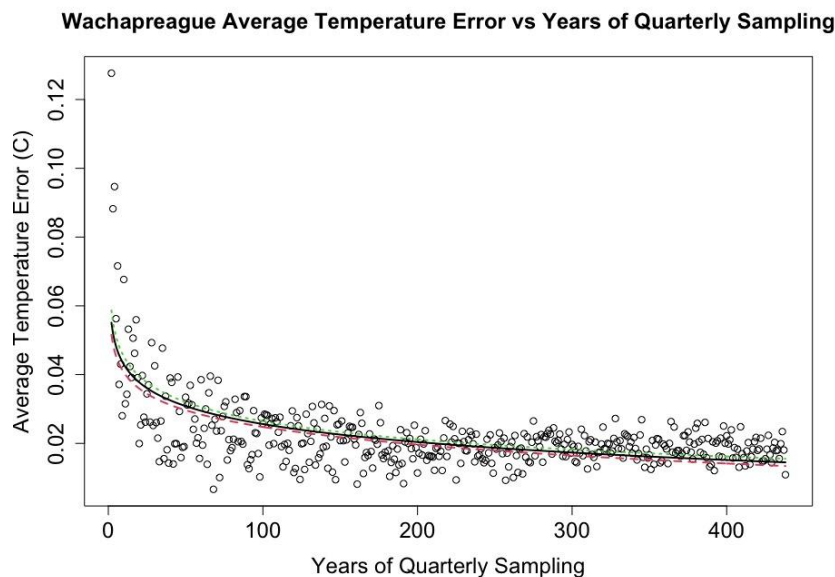


**Figure 13.** Example of logarithmic regression of average error between subsampled and full temperature model versus successive years of quarterly sampling for temperature at site Wachapreague.

In general, it takes all variables at both sites around 25-30 years to reach less than 1% standardized relative change, meaning that if researchers want to decrease the variability in average errors in their models of low frequency observations, they should plan to monitor for at least this long. If they want to reach the plateau, they should plan on monitoring for at least 50-55 years to minimize the variability in average error in their harmonic modeling.

## 5.2 Seasonal High Frequency Anomaly Analysis

### 5.2.1 Positive Anomalies

For site W, salinity had a positive correlation with water level anomalies and a negative correlation with precipitation in winter ( $p=6.00 \times 10^{-6}$  and  $p=0.0108$ ) and spring ( $p=8.00 \times 10^{-5}$  and  $p=1.00 \times 10^{-4}$ ). Predictably, as precipitation increases, surface water is more diluted, lowering salinity. Positive water level anomalies indicate lower than predicted water levels, so increased salinity in these conditions is potentially due to higher evaporation rates leaving behind high saline water. Water level anomalies had a positive relationship with DO in summer

( $p=5.00 \times 10^{-4}$ ) and fall ( $p=.0358$ ), possibly due to shallower water having less stratification and higher gas exchange with the atmosphere, increasing DO concentrations.

For site WW, water level anomalies had a positive correlation with temperature and a negative correlation with salinity in both winter ( $p=0.0201$  and  $p=0.0152$ ) spring ( $p=0.0107$  and  $p=8.00 \times 10^{-4}$ ). Solar radiation is more impactful in shallower water, more effectively elevating water temperature. Higher water levels than expected (negative anomalies) could indicate storm surges and/or a greater tidal flow, increasing salinity.

Both sites had negative correlations between air pressure and temperature in summer ( $p=5.28 \times 10^{-26}$  and  $p=0.0180$ ) and fall ( $p=0.0211$  and  $p=0.0204$ ). Warmer water temperatures decrease air pressure, increasing evaporation and potentially fueling storms (NOAA *Technical*, n.d.). Both sites also had positive correlations between water level anomalies and DO in fall ( $p=0.0358$  and  $p=4.00 \times 10^{-4}$ ), again related to less stratification (Figure 14).

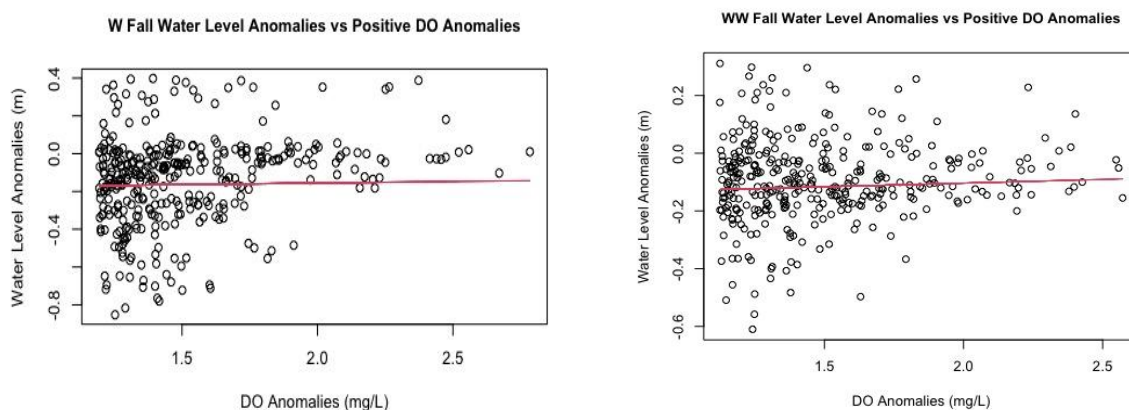


**Figure 14.** Example of positive correlations of positive DO anomalies and water level anomalies at sites W (residual standard error=0.2277) and WW (residual standard error=0.1526).

### 5.2.2 Negative Anomalies

For site W, water level anomalies had a negative correlation with salinity in all 4 seasons ( $p=0.00110$ ,  $1.00 \times 10^{-4}$ ,  $2.00 \times 10^{-5}$ ,  $0.0148$ ). Salinity was lower in higher than expected water,

again likely related to evaporation increasing salinity. This is a temporally strong relationship, occurring in all seasons, so when salinities are lower than expected, they are very impacted by changes in water levels.

Both sites had negative correlations of water level anomalies and salinity in spring ( $p=1.00 \times 10^{-4}$  and  $p=0.0233$ ) and fall ( $p=2.00 \times 10^{-5}$  and  $p=0.0341$ ), likely relating to higher evaporation rates increasing salinity (Figure 15).

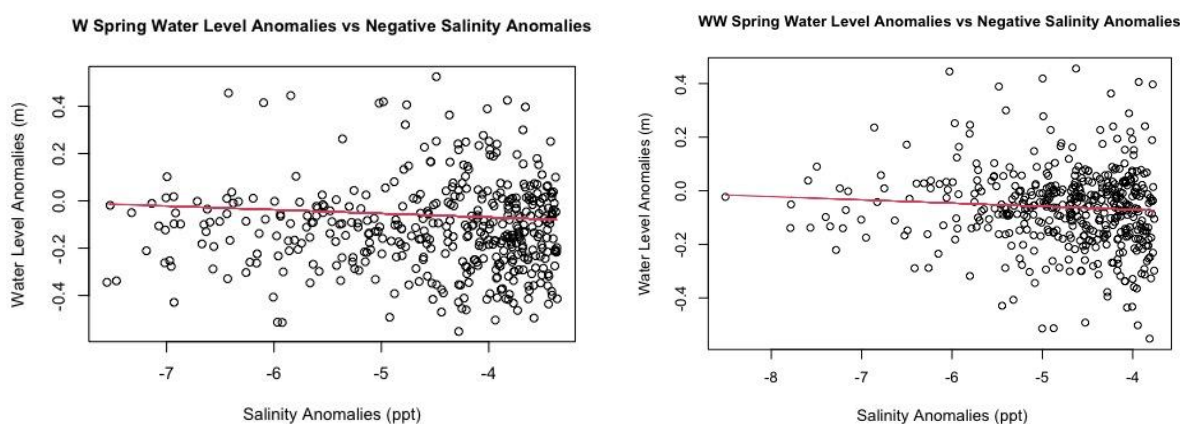


**Figure 15.** Example of negative correlations of negative salinity anomalies and water level anomalies at sites W (residual standard error=0.0784) and WW (residual standard error=0.07933).

### 5.2.3 Summary of Seasonal Anomaly Analysis

In general, temperature, salinity, and DO were the only variables that had repeated significant relationships across both seasons and sites. Salinity increased over time at one high frequency site (W), which could impact future relationships there. All three variables had significant relationships with water level anomalies, and are likely to increase in frequency and magnitude as storm patterns change and sea level rise and saltwater intrusion increase. The significant relationships were seen across seasons, and could increase in severity throughout the year in the future. These relationships are important to examine in order to predict potential changes in water quality due to climate change.

### 5.3 Storm Event High Frequency Anomaly Analysis

#### 5.3.1 Heavy Rain

At site W, heavy rain had a negative correlation between before storm wind speed and temperature on 6/17 ( $p=0.0361$ ) and 7/17 ( $p=0.0497$ ). Increasing winds cause mixing which can decrease surface water temperatures. There was a negative correlation between before storm air pressure and temperature on 9/19/16 ( $0.00332$ ) and 6/21 ( $p=0.0255$ ), as storms that are forming in lower air pressures can use warmer water as fuel. There was a positive correlation between during storm air pressure and temperature on 6/17 ( $p=0.0000658$ ), 8/17 ( $p=0.00516$ ), and 6/21 ( $1.20 \times 10^{-6}$ ). During a storm, there is a co-occurrence of dropping water temperatures and air pressures are rapidly dropping, as mass evaporation cools the surface water. There was a negative correlation with during storm water level anomalies and DO on 9/19/16 ( $p=0.0382$ ) and 10/16 ( $p=9.87 \times 10^{-5}$ ), as when the water is higher than expected, potentially due to the increase in precipitation, rainfall can cause higher saturation of oxygen concentrations (EPA, 2022). There was a negative correlation between during storm precipitation and  $\log_{10}(\text{Chl})$  on 9/19/16 ( $p=0.0151$ ) and 6/17 ( $p=0.0151$ ), as more mixing from rainfall disrupts chlorophyll concentrations. There was a negative correlation with after storm salinity and water level anomalies on 9/28/19 ( $p=0.000438$ ) and 7/17 ( $p=0.0266$ ), as the shallower recovered water has higher salinity than the deeper diluted water. Finally, there was a positive correlation with after storm water level anomalies and  $\log_{10}(\text{Chl})$  on 7/17 ( $p=0.0162$ ) and 3/22 ( $p=0.0102$ ), as the water level returning to normal levels allows for chlorophyll concentrations to rebound and benefit from the potential increase in nutrients brought in.

For site WW, heavy rain had a positive correlation between after storm temperature and water level anomalies on 2/20 ( $p=0.0286$ ) and 3/22 ( $p=0.0476$ ), as the recovered water levels are

shallower and warmer than during the storm. Site WW also had a negative correlation between after storm precipitation and  $\log_{10}(\text{Chl})$  on 2/20 ( $p=0.0351$ ) and 9/20 ( $p=0.0416$ ), as there is less precipitation and mixing after the storm, allowing the chlorophyll concentrations to recover.

### 5.3.2 Tropical Storm

Both sites had positive correlations between during storm air pressure and temperature ( $p=0.0264$  and  $p=0.0495$ ) and after storm precipitation and temperature ( $p=0.000313$  and  $p=0.00376$ ) and negative correlations between during storm water level anomalies and  $\log_{10}(\text{Chl})$  ( $p=0.00775$  and  $p=0.0137$ ) on 9/19 (Figure 16). As mentioned, during storms the air pressure and temperatures are both rapidly dropping, and after the storm the temperature is lower due to the intensity of the tropical storm, taking longer to recover. As the water is elevated during the storm, there can be more nutrients from suspended sediments that can increase the water column chlorophyll concentrations.

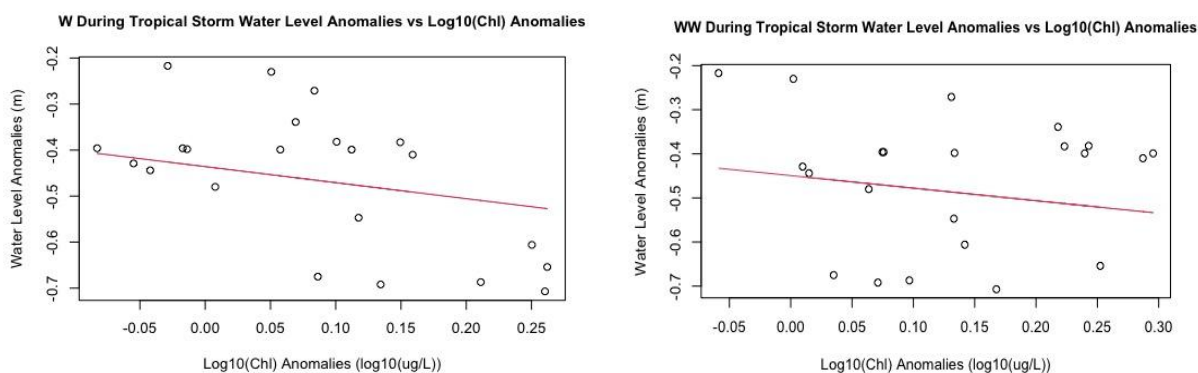


**Figure 16.** Example of negative correlations of during tropical storm  $\log_{10}(\text{Chl})$  anomalies and water level anomalies at sites W (residual standard error=1163) and WW (residual standard error=2191) on 9/19.

### 5.3.3 Hurricane

For site WW, there was a negative correlation between during storm precipitation and temperature on 10/19 ( $p=2.84 \times 10^{-8}$ ) and 7/21 ( $p=0.000584$ ), as increased rainfall during the storm causes mixing that cools the water down.

Both sites had negative correlations between during storm precipitation and temperature ( $p=0.000397$  and  $p=0.000584$ ), and after storm salinity and water level anomalies ( $p=0.00173$  and  $p=0.00412$ ) on 7/21 (Figure 17). As mentioned the more precipitation increases mixing that cools water, and after the storm as the shallower recovered water is higher salinity than diluted water during the storm.

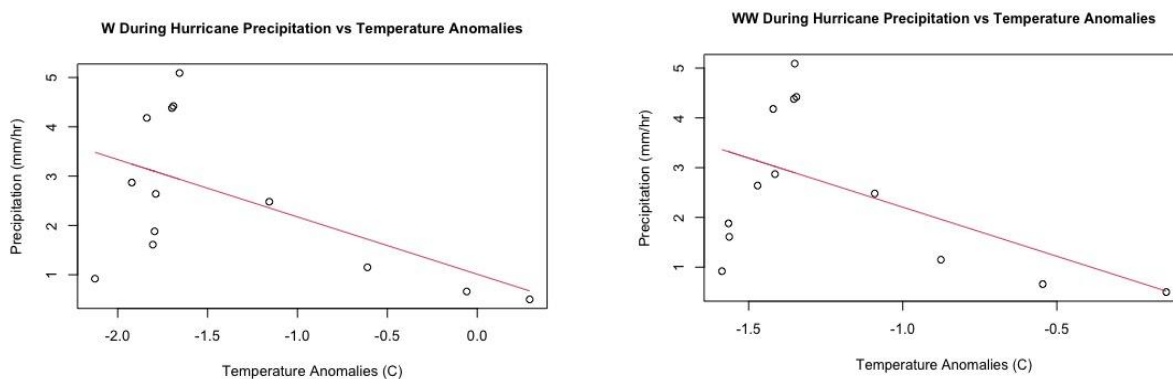


**Figure 17.** Example of negative correlations of during hurricane temperature anomalies and precipitation at sites W (residual standard error=1.331) and WW (residual standard error=1.334) on 7/21.

#### 5.3.4 Coastal Flood

For site W, there was a positive correlation between before storm wind speed and DO on 10/9/21 ( $p=0.0425$ ) and 5/22 ( $p=0.0425$ ), as the higher wind speed causes greater mixing. There was a negative correlation between before storm wind speed and AOU on 10/9/21 ( $p=0.0442$ ) and 10/29/21 ( $p=0.00103$ ), as greater mixing can decrease consumption and respiration. There was a positive correlation with after storm air pressure and temperature on 5/22 ( $p=0.0245$ ) and 9/22 ( $p=0.0451$ ), as the pressure increases after a storm event, so does the temperature as it recovers. There was a negative correlation with after storm wind speed and  $\log_{10}(\text{Chl})$  on 10/29/21 ( $p=0.0164$ ) and 9/22 ( $p=0.00243$ ), as higher winds cause more mixing that can disrupt chlorophyll concentrations.

Across sites, both had positive correlations between before storm DO and wind speed ( $p=0.0424$  and  $p=0.000549$ ), and negative correlations between before storm temperature and precipitation ( $p=0.0121$  and  $p=0.00464$ ), and during storm precipitation with salinity ( $p=0.0439$  and  $p=0.000119$ ) and DO ( $p=0.0113$  and  $p=0.00404$ ) on 5/22 (Figure 18). Increased winds cause mixing which increases DO, and as precipitation increases approaching a storm, temperatures decrease. Increased precipitation during a storm dilutes the water and lowers salinity. Both sites had positive correlations between before storm precipitation with temperature ( $p=1.08 \times 10^{-6}$  and  $p=0.000923$ ) and  $\log_{10}(\text{Chl})$  ( $p=0.0108$  and  $p=0.000140$ ) on 9/22. Interestingly this is the opposite relationship as 5/22, and could be related to a stronger storm system of warmer water that impacted this flood or the season, as this storm occurred in the spring. The chlorophyll concentrations increasing before the flood could be related to resuspension of sediments.

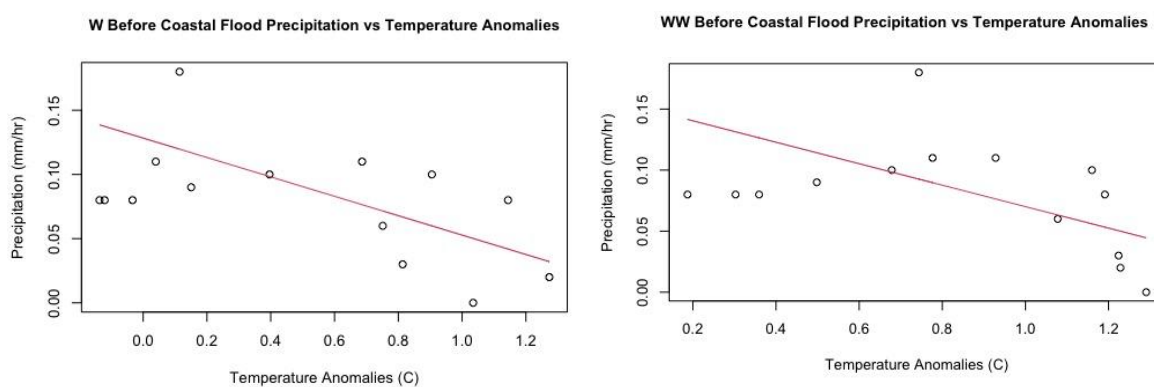


**Figure 18.** Example of negative correlations of before coastal flood temperature anomalies and precipitation at sites W (residual standard error=0.05280) and WW (residual standard error=0.5122) on 5/22.

### 5.3.5 Winter Storm

For site W, there was a negative correlation between after storm salinity and water level anomalies on 12/20 ( $p=0.0188$ ) and 1/22 ( $p=0.00758$ ), as the shallower water is more salinated. There was a positive correlation between after storm AOU and water level anomalies 12/20

( $p=0.000800$ ) and  $1/22$  ( $p=0.00349$ ), as deeper storm surge water is likely to be more turbid and faster moving, limiting consumption.

### *5.3.6 Cross Storms and Sites*

Across storms and sites, there was a negative correlation between before storm precipitation and temperature in heavy rain, tropical storms, and coastal floods, as these storms have massive amounts of precipitation and high wind speeds that can cause the temperature to rapidly drop beforehand. There was a negative correlation between during storm water level anomalies and  $\log_{10}(\text{Chl})$  in tropical storms, hurricanes, and coastal floods as the mixing of nutrients from deeper water and resuspension of sediments could cause elevated levels of chlorophyll. There was a positive correlation between during storm air pressure and temperature in heavy rain, tropical storms, and winter storms, as mentioned both the temperature and air pressure are rapidly dropping during the storm event. There was a negative correlation between during storm precipitation and salinity in tropical storms, hurricanes, coastal floods, winter storms, as the increase in rain dilutes the salinity. There was a negative correlation between during storm precipitation and  $\log_{10}(\text{Chl})$  in heavy rain, tropical storms, and hurricanes, as more precipitation can increase mixing and dilute the concentrations. There was a negative correlation between after storm water level anomalies and salinity in all storm events, the most widespread relationship, as the shallower water is more salty than deeper diluted water. Finally, there was a negative correlation between after storm precipitation and DO in heavy rain, coastal floods, and winter storms, as when the rain slows down there is less saturation via rainfall and the DO is not as elevated.

### *5.3.7 Summary of Storm Anomaly Analysis*

Repeated significant relationships are seen across all storm types. Specifically, the cross site types relationships were restricted to tropical storms, coastal floods, and hurricanes, which are the more intense storm types that can cause higher threat to coastal infrastructures and human lives. The variables in those relationships are temperature, salinity, and DO, also seen in seasonal, and  $\log_{10}(\text{Chl})$ , and these relationships occurred most during the storms. Additionally, salinity has been found to be increasing and  $\log_{10}(\text{Chl})$  has been found to be decreasing over time at the high frequency sites, which could impact future relationships. Specifically, temperature had the most significant relationships, however these baseline temperatures are likely to increase in the near future, potentially impacting these relationships. Across storm and site types however, including all storms, had the same 4 variables of temperature, salinity, DO, and  $\log_{10}(\text{Chl})$ . In both of these relationships, precipitation had the most significant relationships. As precipitation intensity is likely to increase in the future, more severe and more potential relationships with precipitation could develop.

## 6. Summary

Water quality is a vital metric to measuring the status of a body of water, especially in coastal areas. Strong seasonal patterns are seen in all water quality variables in both the high and low frequency sites. For temperature, DO, and AOU, all sites are dominated by the first harmonic, indicating one peak per year, while salinity and  $\log_{10}(\text{Chl})$  have a mix of dominating harmonics between sites and site types. Sites near the ocean or more inland generally show more cohesiveness within their geographical types, with the exception of salinity at the inland sites. The differences in salinity are likely related to higher environmental variability and seasonal changes in freshwater inflow and depths at these land adjacent sites. When subsampling the high

frequency sites at the rate of low frequency inland measurements, they tend to show relatively low percent differences, with salinity at site W and AOU at site WW being the only two variables over 1% percent difference. This indicates that the VCR's consistency of measurements estimated seasonal cycles well due to the long term (up to 30 years) data sets.

For long term changes, an increase in  $\log_{10}(\text{Chl})$  was the most frequent trend, followed by increase in salinity, temperature, and decrease in AOU, with DO not having any long term changes at any sites. At the 2 high frequency sites, site WW had opposite relationship with  $\log_{10}(\text{Chl})$  (negative) and site W with AOU (positive), likely related to their higher frequency monitoring having more noise and catching smaller variations, as well as shorter time frames of measurements (4-6 years). These changes indicate that these variables are not static, and consistent and continual monitoring must be in place to mitigate long term negative effects.

In simulating quarterly sampling, there was high variability in error between years in the first 5-15 years, indicating sites with that minimal of data availability are not the best option for harmonic analysis on a low frequency scale. The variables took about 25-30 years to reach less than 1% standardized relative change, and over 50 to plateau around less than 0.25% standardized relative change. This indicates that 25 years is adequate enough to model using harmonic analysis, but at least 50 years of data is required to reach a plateau .

Focusing on the high frequency sites anomalies, on a seasonal scale there were repeated significant relationships with the variables of temperature, salinity, and DO. As mentioned at site W salinity e increased, which could impact these relationships in the future. All seasons had at least one significant relationship, indicating this could be a year round issue that is likely to be exacerbated by climate change. Water level anomalies had the most frequent significant

relationships, again, a factor that is likely to become more frequently severe as storm surges are larger and more frequent and sea level rise and salt water intrusion becomes more severe.

On a storm scale, across both sites W and WW, tropical storms, coastal floods, and hurricanes had the only significant relationships with temperature, salinity, DO, and  $\log_{10}(\text{Chl})$ . These were most frequently with precipitation, which is likely to become more frequent and intense in a changing climate. Across both sites W and WW and all storm types, the same variables had significant relationships across all storm types, the most frequent being tropical storms, an intense and potentially life threatening storm to people residing in coastal areas. Again, the most frequent relationship was with precipitation, which is likely to increase in both intensity and frequency.

## **7. Conclusions and Future Directions**

Using harmonic analysis, temperature, salinity, DO,  $\log_{10}(\text{Chl})$ , and AOU show strong seasonality and variation on a temporal and spatial scale. These changes are driven by climatic factors, both of which are likely to change in the near future due to anthropogenic influences. All variables except for DO had long term changes over time using GLS, indicating these are not stable and instead likely to be under increasing pressure to change as the environment changes. Simulating quarterly sampling of these variables, 25 years are needed to limit the variability in error (less than 1% standardized relative change between years), and ideally over 50 will cause a plateau (less than 0.25% standardized relative change between years). The VCR has long term water quality data sets that range up to 30 years, indicating that they have hit the below 1% standardized relative change threshold and are doing a relatively good job limiting error variability, and will continue to be more accurate as more years are collected. This is important

information as it guides researchers establishing water quality monitoring sites as well as how many years of sampling they should plan on having to have the most accurate model of seasonal patterns using harmonic analysis. This can be expanded to water quality variables that are not yet measured or just beginning to be measured at long term low frequency sites, using a reference high frequency station nearby if available.

Results show that high frequency sites' water quality anomalies have significant relationships with both seasons and storms that are not limited to singular seasons or storm types. For seasons, temperature, salinity, and DO had the most frequent significant relationships, especially with water level anomalies, which large negative values can be indicative of potential storm surges. As storminess increases in frequency, these relationships could become more pronounced and common and have adverse impacts on water quality. Future work could involve breaking down seasonal analysis by year and/or season and seeing if these trends are still significant. For storms, temperature, salinity, DO, and  $\log_{10}(\text{Chl})$  were the most common significant relationships across storm type and site type, with  $\log_{10}(\text{Chl})$  and salinity the high frequency sites over time. These most commonly were significant with precipitation, which again is likely to increase with increasing storminess. Future research could investigate if similar relationships are seen at different high frequency water quality sites, as well as at other high frequency water quality sites with longer data availability and less gaps that would allow for more storm events to be captured. Additionally, sites that are not just in coastal waters, such as lakes or inland streams, could also be monitored during storm events. These results are important to recognize in the face of climate change, and serve as a starting point for specific analysis on water quality anomalies in terms of seasons and storms.

## 8. Appendix

**Table A1.** VCR and VIMS Sites Temperature Composite Harmonic Wave Elements

Site	$pV_1$	$pV_2$	$t_{min}$	Min value	$t_{max}$	Max value	$A_{max}$	$\chi_v^2$
RBCM	91.44	8.559	19.04 ± 0.7691	6.532 ± 0.1174	213.4 ± 0.6246	30.18 ± 0.1091	11.81 ± 0.07356	0.1083
CCM	96.28	3.715	22.80 ± 0.5017	5.468 ± 0.06067	216.0 ± 0.4252	27.34 ± 0.0702	10.94 ± 0.04239	0.1018
LCI	94.14	5.862	27.76 ± 0.5349	4.381 ± 0.08229	218.1 ± 0.6020	27.48 ± 0.07845	11.55 ± 0.05199	0.06501
MI	96.32	3.680	26.02 ± 0.5049	5.132 ± 0.07037	219.6 ± 0.5029	27.46 ± 0.07568	11.16 ± 0.04807	0.08747
NM	94.42	5.581	22.22 ± 0.5822	4.781 ± 0.08964	216.9 ± 0.5823	28.46 ± 0.09455	11.84 ± 0.05997	0.08183
OH	95.46	4.542	17.56 ± 0.4370	6.132 ± 0.06949	215.1 ± 0.3944	29.34 ± 0.06913	11.61 ± 0.04472	0.09989
PCM	95.87	4.126	14.78 ± 0.4819	5.653 ± 0.07131	213.2 ± 0.4378	29.33 ± 0.08099	11.84 ± 0.04904	0.1217
QI	97.27	2.727	28.95 ± 0.4210	5.020 ± 0.05600	219.3 ± 0.3908	26.18 ± 0.0526	10.58 ± 0.03692	0.0819
RB	95.89	4.114	20.37 ± 0.4196	5.161 ± 0.06246	213.4 ± 0.3823	28.69 ± 0.06209	11.76 ± 0.04317	0.08472
RCC	94.39	5.610	22.52 ± 0.5069	4.898 ± 0.09308	216.3 ± 0.5525	28.45 ± 0.08594	11.77 ± 0.05637	0.07222
SH	95.58	4.419	22.03 ± 0.4687	5.257 ± 0.07630	218.4 ± 0.5073	27.81 ± 0.06847	11.28 ± 0.04967	0.09725
SHS	92.16	7.844	23.45 ± 0.7004	5.605 ± 0.09962	215.8 ± 0.6257	28.63 ± 0.08999	11.53 ± 0.05907	0.08948
SS	94.10	5.896	28.50 ± 0.5318	4.268 ± 0.08045	222.7 ± 0.5615	26.71 ± 0.08535	11.22 ± 0.05678	0.06800
W (Full)	99.39	0.6067	19.01	5.287	212.2	28.76	11.74	0.07591
W (Sub)			18.74 ± 0.3700	5.264 ± 0.06006	212.3 ± 0.2966	28.79 ± 0.03789	11.76 ± 0.03228	
WW (Full)	99.78	0.2227	16.49	6.011	211.8	29.66	11.82	0.06268
WW (Sub)			16.73 ± 0.3311	6.004 ± 0.05897	211.7 ± 0.3177	29.69 ± 0.03664	11.84 ± 0.03291	

Where  $pV_1$ (%) is the percent variance of the first harmonic,  $pV_2$ (%) is the percent variance of the second harmonic,  $t_{min}$  (days)

is the date of minimum value ( $^{\circ}\text{C}$ ),  $t_{max}$  (days) is the date of the maximum value ( $^{\circ}\text{C}$ ), and  $A_{max}$  ( $^{\circ}\text{C}$ ) is the amplitude.

**Table A2.** VCR and VIMS Sites Salinity Composite Harmonic Wave Elements

Site	$pV_1$	$pV_2$	$t_{min}$	Min value	$t_{max}$	Max value	$A_{max}$	$\chi_v^2$
RBCM	66.90	33.10	$330.3 \pm 2.409$	$29.05 \pm 0.09615$	$212.4 \pm 2.830$	$31.98 \pm 0.08480$	$1.499 \pm 0.0746$	0.9007
CCM	27.97	72.03	$44.71 \pm 3.452$	$30.28 \pm 0.03983$	$303.4 \pm 3.178$	$31.38 \pm 0.03994$	$0.5538 \pm 0.03045$	0.9937
LCI	24.60	75.40	$312.1 \pm 2.843$	$30.64 \pm 0.03930$	$219.0 \pm 3.416$	$31.57 \pm 0.04745$	$0.4801 \pm 0.03338$	0.9851
MI	57.91	42.09	$56.60 \pm 4.952$	$30.88 \pm 0.03830$	$165.4 \pm 4.769$	$31.60 \pm 0.3582$	$0.3720 \pm 0.02716$	1.021
NM	54.35	45.65	$329.7 \pm 4.672$	$30.80 \pm 0.40949$	$213.1 \pm 5.833$	$31.56 \pm 0.03960$	$0.3874 \pm 0.02971$	1.024
OH	59.27	40.73	$32.91 \pm 3.257$	$28.83 \pm 0.07342$	$280.7 \pm 4.672$	$30.24 \pm 0.6832$	$0.7370 \pm 0.05587$	1.007
PCM	85.15	14.85	$61.45 \pm 2.131$	$24.46 \pm 0.1108$	$202.4 \pm 4.084$	$29.57 \pm 0.1185$	$2.552 \pm 0.08339$	0.9064
QI	60.61	39.39	$48.66 \pm 3.392$	$30.13 \pm 0.04619$	$293.5 \pm 4.655$	$31.28 \pm 0.04663$	$0.5923 \pm 0.031646$	1.004
RB	95.76	4.237	$53.84 \pm 3.359$	$28.82 \pm 0.05784$	$277.4 \pm 4.300$	$30.76 \pm 0.06416$	$0.9721 \pm 0.04440$	0.9677
RCC	65.33	34.67	$320.4 \pm 4.153$	$30.75 \pm 0.03464$	$206.9 \pm 5.759$	$31.47 \pm 0.03595$	$0.3642 \pm 0.02800$	1.030
SH	22.40	77.60	$40.31 \pm 3.584$	$30.76 \pm 0.03988$	$292.6 \pm 4.848$	$31.53 \pm 0.03732$	$0.4035 \pm 0.02640$	1.019
SHS	44.92	55.08	$308.3 \pm 4.731$	$30.62 \pm 0.05266$	$61.55 \pm 5.755$	$31.61 \pm 0.05263$	$0.5067 \pm 0.03628$	1.032
SS	17.17	82.83	$303.7 \pm 4.444$	$30.93 \pm 0.03317$	$202.9 \pm 4.980$	$31.56 \pm 0.03148$	$0.3205 \pm 0.02601$	1.025
W (Full)	94.62	5.384	46.49	28.76	186.4	31.59	1.417	0.7926
W (Sub-sampled)			$46.17 \pm 1.206$	$28.71 \pm 0.04501$	$192.2 \pm 2.710$	$31.7 \pm 0.03434$	$1.479 \pm 0.02907$	
WW (Full)	95.48	4.515	57.67	25.20	215.6	32.49	3.646	0.3573

WW (Sub-sampled)	57.23 ± 0.6475	25.21 ± 0.05455	218.1 ± 1.941	32.49 ± 0.03267	3.636 ± 0.02890
---------------------	-------------------	--------------------	------------------	--------------------	--------------------

Where  $pV_1$  (%) is the percent variance of the first harmonic,  $pV_2$  (%) is the percent variance of the second harmonic,  $t_{min}$  (days) is the date of minimum value (ppt),  $t_{max}$  (days) is the date of the maximum value (ppt), and  $A_{max}$  (ppt) is the amplitude.

**Table A3.** VCR and VIMS Sites DO Composite Harmonic Wave Elements

Site	$pV_1$	$pV_2$	$t_{min}$	Min value	$t_{max}$	Max value	$A_{max}$	$\chi_v^2$
RBCM	98.25	1.750	223.0 ± 4.303	6.1537 ± 0.06486	25.00 ± 1.197	11.15 ± 0.07013	2.499 ± 0.04633	0.5741
CCM	97.91	2.088	213.4 ± 1.552	5.108 ± 0.04066	32.49 ± 1.000	10.46 ± 0.04011	2.679 ± 0.02736	0.4291
LCI	97.45	2.549	214.7 ± 3.284	6.448 ± 0.05632	36.90 ± 1.369	11.74 ± 0.06213	2.648 ± 0.03778	0.4352
MI	99.81	0.1885	225.6 ± 3.178	6.257 ± 0.04758	31.38 ± 1.095	10.84 ± 0.05075	2.291 ± 0.03301	0.5156
NM	98.44	1.555	219.6 ± 2.723	5.658 ± 0.05179	29.80 ± 0.9734	11.66 ± 0.05282	3.003 ± 0.03457	0.3307
OH	99.74	0.2632	236.9 ± 3.439	6.228 ± 0.04122	30.03 ± 1.547	10.93 ± 0.05597	2.352 ± 0.03523	0.5498
PCM	99.81	0.1947	208.9 ± 2.973	4.916 ± 3.439	26.31 ± 0.7929	10.36 ± 0.04174	2.721 ± 0.02871	0.4735
QI	98.82	1.175	209.3 ± 2.393	6.265 ± 0.03695	31.46 ± 1.073	10.74 ± 0.04051	2.238 ± 0.02600	0.5216
RB	98.95	1.053	206.2 ± 2.318	5.496 ± 0.03927	26.99 ± 0.9468	10.41 ± 0.03748	2.460 ± 0.02400	0.4836
RCC	97.01	2.987	222.9 ± 2.303	5.849 ± 0.05174	26.81 ± 1.130	11.21 ± 0.0542	2.680 ± 0.03693	0.3677
SH	99.59	0.4093	217.6 ± 3.412	6.072 ± 0.06580	24.71 ± 1.080	11.05 ± 0.05189	2.500 ± 0.03320	0.5116
SHS	95.49	4.512	225.1 ± 2.383	6.382 ± 0.0543	21.08 ± 1.300	11.18 ± 0.05252	2.401 ± 3.412	0.4231
SS	96.30	3.701	217.9 ± 3.045	6.555 ± 0.05671	35.49 ± 1.441	11.97 ± 0.06018	2.709 ± 0.04209	0.4352
W (Full)	99.99	0.002216	205.8	5.184	24.81	10.38	2.597	0.1095
W (Sub-sampled)			211.0	4.920 ± 0.3173	24.07 ± 0.007157	10.53 ± 0.009804	2.808 ± 0.005677	

mpled)

WW (Full)	99.49	0.5102	205.8	5.184	24.81	10.38	2.597	0.1203
WW (Sub-sampled)			205.8 ± 0.6926	5.172 ± 0.01413	24.81 ± 0.3786	10.38 ± 0.02070	2.605 ± 0.01170	

Where  $pV_1$  (%) is the percent variance of the first harmonic,  $pV_2$  (%) is the percent variance of the second harmonic,  $t_{min}$  (days) is the date of minimum value (mg/L),  $t_{max}$  (days) is the date of the maximum value (mg/L), and  $A_{max}$  (mg/L) is the amplitude.

**Table A4.** VCR and VIMS Sites Log10(Chl) Composite Harmonic Wave Elements

Site	$pV_1$	$pV_2$	$t_{min}$	Min value	$t_{max}$	Max value	$A_{max}$	$\chi_v^2$
RBCM	56.61	43.39	333.1 ± 1.491	0.4664 ± 0.01185	221.2 ± 1.400	1.094 ± 0.01208	0.3148 ± 0.01030	0.6365
CCM	46.10	53.90	322.3 ± 1.611	0.3899 ± 0.007790	216.0 ± 1.152	0.7212 ± 0.007552	0.1680 ± 0.006534	0.8369
LCI	67.57	32.43	110.2 ± 3.463	0.5783 ± 0.01066	235.2 ± 3.6811	0.8897 ± 0.009757	0.1559 ± 0.007786	0.8947
MI	53.56	46.44	117.3 ± 1.970	0.5071 ± 0.009190	230.3 ± 2.116	0.8782 ± 0.01015	0.1842 ± 0.007861	0.8818
NM	28.11	71.89	122.9 ± 2.741	0.5102 ± 0.009866	228.4 ± 2.936	0.7595 ± 0.01070	0.1283 ± 0.007851	0.9391
OH	83.20	16.80	340.1 ± 3.687	0.1438 ± 0.01223	205.3 ± 1.065	0.9942 ± 0.01155	0.4340 ± 0.008547	0.6572
PCM	61.43	38.57	325.4 ± 2.447	0.3969 ± 0.008387	201.1 ± 0.8110	1.087 ± 0.008149	0.3442 ± 0.006431	0.6590
QI	32.38	67.62	110.5 ± 1.698	0.5456 ± 0.007712	215.9 ± 1.602	0.8145 ± 0.007954	0.1340 ± 0.005924	0.9407
RB	44.95	55.05	323.1 ± 2.334	0.4420 ± 0.008683	212.4 ± 2.083	0.7312 ± 0.008219	0.1432 ± 0.007042	0.9485
RCC	49.06	50.94	115.6 ± 2.640	0.4999 ± 0.01068	228.4 ± 2.588	0.8665 ± 0.01205	0.1819 ± 0.009311	0.8466
SH	50.23	49.77	322.3 ± 1.495	0.3945 ± 0.008537	215.7 ± 0.9116	0.8686 ± 0.008528	0.2375 ± 0.007217	0.7142
SHS	51.43	48.57	320.9 ± 2.320	0.6154 ± 0.01061	211.4 ± 1.429	1.022 ± 0.01095	0.2051 ± 0.008813	0.7113
SS	74.58	25.44	117.5 ± 3.218	0.5805 ± 0.01208	323.5 ± 4.955	0.8843 ± 0.01927	0.1748 ± 0.01567	0.9384

W (Full)	52.41	47.59	326.7	0.4392	221.3	1.102	0.3316	0.4550
W (Sub-sampled)			315.2 ± 0.2259	0.3048 ± 0.003282	205.6 ± 0.1821	1.066 ± 0.001977	0.3810 ± 0.002348	
WW (Full)	38.52	61.48	326.7	0.4392	221.3	1.102	0.3316	0.5848
WW (Sub-sampled)			326.6 ± 0.5477	0.4347 ± 0.006014	220.8 ± 0.4685	1.106 ± 0.005657	0.3352 ± 0.004869	

Where  $pV_1$  (%) is the percent variance of the first harmonic,  $pV_2$  (%) is the percent variance of the second harmonic,  $t_{min}$  (days) is the date of minimum value ( $\log_{10}(\text{ug/L})$ ),  $t_{max}$  (days) is the date of the maximum value ( $\log_{10}(\text{ug/L})$ ), and  $A_{max}$  ( $\log_{10}(\text{ug/L})$ ) is the amplitude.

**Table A5.** VCR and VIMS Sites AOU Composite Harmonic Wave Elements

Site	$pV_1$	$pV_2$	$t_{min}$	Min value	$t_{max}$	Max value	$A_{max}$	$\chi_v^2$
RBCM	85.23	14.77	37.29 ± 2.514	-1.117 ± 0.05464	277.9 ± 4.538	0.6904 ± 0.04950	0.9092 ± 0.03655	0.9572
CCM	94.57	5.427	40.87 ± 3.165	-0.3479 ± 0.04028	210.6 ± 4.600	1.630 ± 0.04602	0.9924 ± 0.03533	0.8207
LCI	98.61	1.386	49.67 ± 3.898	-1.165 ± 0.06360	196.0 ± 5.368	0.2480 ± 0.06432	0.7110 ± 0.04349	0.9880
MI	90.00	10.00	37.42 ± 2.876	-0.6943 ± 0.03904	171.7 ± 4.591	0.5796 ± 0.03768	0.6393 ± 0.02845	0.9768
NM	87.05	12.95	46.25 ± 3.999	-0.6580 ± 0.05469	225.3 ± 3.4682	1.079 ± 0.04981	0.8532 ± 0.03697	0.8513
OH	78.08	21.92	32.81 ± 2.567	-0.7930 ± 0.04129	276.1 ± 3.328	0.6336 ± 0.03724	0.7170 ± 0.02927	0.9713
PCM	92.15	7.845	37.12 ± 1.885	0.07197 ± 0.04003	272.1 ± 4.064	1.771 ± 0.03498	0.8594 ± 0.02695	0.9137
QI	85.50	14.50	44.17 ± 3.005	-0.4531 ± 0.03544	175.3 ± 3.539	0.6787 ± 0.03140	0.5679 ± 0.02639	0.9537
RB	99.79	0.2111	26.96 ± 3.462	-0.2934 ± 0.4979	221.7 ± 5.092	1.173 ± 0.03443	0.7328 ± 3.005	0.9018
RCC	88.49	11.51	46.28 ± 4.365	-0.6578 ± 0.06532	242.0 ± 3.501	0.8668 ± 0.04798	0.7529 ± 0.03865	0.9110
SH	97.51	2.494	24.69 ± 2.610	-1.002 ± 0.04500	250.5 ± 3.763	0.6890 ± 0.03763	0.8458 ± 0.03311	0.9040

SHS	96.70	3.299	47.47 ± 4.967	-0.6984 ± 0.05998	246.8 ± 4.671	0.1307 ± 0.06234	0.4310 ± 0.03915	1.035
SS	92.57	7.434	55.67 ± 4.562	-1.080 ± 0.06136	219.9 ± 4.911	0.03939 ± 0.06920	0.5627 ± 0.04299	1.005
W (Full)	98.50	1.500	37.98	-0.09267	201.0	1.539	0.8157	0.4104
W (Sub-sampled)			37.45 ± 0.7903	-0.1042 ± 0.01197	201.7 ± 1.212	1.539 ± 0.01250	0.8215 ± 0.008081	
WW (Full)	97.49	2.51	34.37	0.07480	190.2	1.227	0.5759	0.6316
WW (Sub-sampled)			34.03 ± 1.362	0.07031 ± 0.01430	194.2 ± 3.012	1.232 ± 0.01873	0.5808 ± 0.01155	

Where  $pV_1(\%)$  is the percent variance of the first harmonic,  $pV_2(\%)$  is the percent variance of the second harmonic,  $t_{min}$  (days) is the date of minimum value (mg/L),  $t_{max}$  (days) is the date of the maximum value (mg/L), and  $A_{max}$  (mg/L) is the amplitude.

**Table A6.** Percent Differences between Full and Subsampled High Frequency Sites

Site	Parameter	Min/Max Date (%)	Min/Max (%)	Amplitude (%)	Overall Average (%)
W	Temperature	0.01518	0.09329	0.2262	0.1115
	Salinity	3.107	0.2823	4.286	2.558
	DO	0.1506	0.3843	0.1152	0.2167
	Log10(Chl)	0.1284	0.1409	0.3149	0.1948
	AOU	0.3439	0.01175	0.7171	0.3576
WW	Temperature	0.01247	0.1018	0.1613	0.09185
	Salinity	1.147	0.005413	0.2588	0.4703
	DO	0.01641	0.2348	0.3058	0.1857
	Log10(Chl)	0.2068	0.3235	1.095	0.5417
	AOU	2.105	0.4970	0.8434	1.149

**Table A7.** Significant Long Term Changes in Water Quality Parameters

Parameter	Site	Rate of Change
Temperature	RBCM	0.07497 °C/year
	PCM	0.06771 °C/year
	RB	0.05249 °C/year
Salinity	CCM	0.06723 ppt/year
	OH	0.08015 ppt/year
	PCM	0.09906 ppt/year
	QI	0.06781 ppt/year
	RB	0.07490 ppt/year
	W	0.2890 ppt/year
Log10(Chl)	RBCM	0.01191 log10(ug/L)/year
	MI	0.01851 log10(ug/L)/year
	PCM	0.009720 log10(ug/L)/year
	QI	0.008537 log10(ug/L)/year
	RB	0.009563 log10(ug/L)/year
	RCC	0.01865 log10(ug/L)/year
	SH	0.01787 log10(ug/L)/year
	WW	-0.06924 log10(ug/L)/year
AOU	RBCM	-0.0565 mg/L/year
	SH	-0.04413 mg/L/year
	W	0.04180 mg/L/year

**Table A8.** W and WW Years of Quarterly Data Sampling Average Difference

Site	Parameter	Standardized Relative Change	Years to Reach	Average Difference
W	Temperature	1	29	0.03495 °C

		0.5	45	0.03164 °C
		.25	62	0.02922 °C
	Salinity	1	25	0.05068 ppt
		0.5	39	0.04949 ppt
		.25	54	0.04862 ppt
	DO	1	27	0.01648 mg/L
		0.5	42	0.01572 mg/L
		0.25	57	0.01520 mg/L
	Log10(Chl)	1	24	0.01307 log10(ug/L)
		0.5	37	0.01303 log10(ug/L)
		0.25	51	0.01301 log10(ug/L)
	AOU	1	25	0.01308 mg/L
		0.5	39	0.01283 mg/L
		0.25	53	0.01265 mg/L
WW	Temperature	1	25	0.03434 °C
		0.5	39	0.03132 °C
		.25	54	0.02911 °C
	Salinity	1	25	0.02959 ppt
		0.5	35	0.02543 ppt
		.25	44	0.02294 ppt
	DO	1	24	0.01254 mg/L
		0.5	38	0.01176 mg/L
		0.25	51	0.01126 mg/L
	Log10(Chl)	1	25	0.004710

				log10(ug/L)
		0.5	39	0.004310
				log10(ug/L)
		0.25	53	0.004035
				log10(ug/L)
	AOU	1	26	0.01102 mg/L
		0.5	40	0.009916 mg/L
		0.25	54	0.009144 mg/L

**Table A9.** W and WW Years of Quarterly Data Sampling Average Percent Difference

Site	Parameter	Standardized Relative Change	Years to Reach	Average Percent Difference
W	Temperature	1	29	0.1327 %
		0.5	45	0.1198 %
		.25	62	0.1105 %
	Salinity	1	24	1.900 %
		0.5	37	1.892 %
		.25	51	1.885 %
	DO	1	27	0.3120 %
		0.5	43	0.2920 %
		0.25	59	0.2785 %
	Log10(Chl)	1	24	1.331 %
		0.5	37	1.328 %
		0.25	51	1.326 %
	AOU	1	26	0.8067 %
		0.5	40	0.7849 %
		0.25	54	0.7697 %
WW	Temperature	1	26	0.1360 %

	0.5	40	0.1220 %
	.25	54	0.1122 %
Salinity	1	23	0.3703 %
	0.5	33	0.3249 %
	.25	42	0.2963 %
DO	1	22	0.7503 %
	0.5	34	0.7409 %
	0.25	46	0.7344 %
Log10(Chl)	1	25	0.5296 %
	0.5	38	0.4976 %
	0.25	52	0.4737 %
AOU	1	26	1.150 %
	0.5	40	1.044 %
	0.25	54	0.9690 %

## 9. References

- Anthony A., Atwood, J., August, P., Byron, C., Cobb, S., Foster, C., Fry, C., Gold, A., Hagos, K., Heffner, L., Kellogg, D. Q., Lellis-Dibble, K., Opaluch, J. J., Oviatt, C., Pfeiffer-Herbert, A., Rohr, N., Smith, L., Smythe, T., Swift, J., & Vinhaterio, N. (2009). Coastal Lagoons and Climate Change: Ecological and Social Ramifications in U.S. Atlantic and Gulf Coast Ecosystems. *Ecology and Society*, *14*(1), Retrieved August 23, 2022, from <https://www.jstor.org/stable/26268055>
- Benyahya, L., Caissie, D., St-Hilaire, A., Ouarda, T. B. M. J., & Bobee, B. (2007). A Review of Statistical Water Temperature Models. *Canadian Water & Resources Journal*, *32*(3). 179-192. <https://doi.org/10.4296/cwrj3203179>
- Biological & Chemical Oceanography Data Management Office (n.d.). *Parameter: Apparent Oxygen Utilization*. Retrieved August 23, 2022 from <https://www.bco-dmo.org/parameter/527499#:~:text=In%20freshwater%20or%20marine%20systems.same%20physical%20and%20chemical%20properties>
- Boyer, T., Conkright, M. E., & Levitus, S. (1999). Seasonal Variability of dissolved oxygen, percent oxygen saturation, and apparent oxygen utilization in the Atlantic and Pacific Ocean. *Deep Sea Research Part I: Oceanographic Research Papers*, *46*(9), 1593-1613. [https://doi.org/10.1016/S0967-0637\(99\)00021-7](https://doi.org/10.1016/S0967-0637(99)00021-7)
- Boyer, J. N., Keble, C. R., Ortner, P. B., & Rudnick, D. T. (2009). Phytoplankton bloom status: Chlorophyll a biomass as an indicator of water quality condition in the southern estuaries of Florida, USA. *Ecological Indicators*, *9*(6), S56-S67. <https://doi.org/10.1016/j.ecolind.2008.11.013>

- Briciu-Burghina, C., Sullivan, T., Chapman, J., & Regan, F. (2014). Continuous high-frequency monitoring of estuarine water quality as a decision support tool: a Dublin Port case study. *Environmental Monitoring and Assessment*, 186, 5561-5580.  
<https://doi.org/10.1007/s10661-014-3803-9>
- Brown, L. E. & Hannah, D. M. (2007). Alpine Stream Temperature Response to Storm Events. *Journal of Hydrometeorology*, 8(4), 952-967. <https://doi.org/10.1175/JHM597.1>
- Bugica, K., Sterba-Boatwright, B., & Wetz, M. S. (2020). Water quality trends in Texas Estuaries. *Marine Pollution Bulletin*, 152, 110903.  
<https://doi.org/10.1016/j.marpolbul.2020.110903>
- Bukaveckas, P. A., Tassone, S., Lee, W., & Franklin, R. B. (2020). The Influence of Storm Events on Metabolism and Water Quality of Riverine and Estuarine Segments of the James, Mattaponi, and Pamunkey Rivers. *Estuaries and Coasts*, 43, 1585-1602.  
<https://doi.org/10.1007/s12237-020-00819-9>
- Burroughs, Q. J. (2003). *Weather Cycles: Real or Imaginary?* (2nd ed.). Cambridge University Press.
- Burt, T.P., Howden, N. J. K., & Worrall, F. (2014). On the importance of very long-term water quality records. *Wiley Interdisciplinary Reviews Water*, 1(1), 41-48.  
<https://doi.org/10.1002/wat2.1001>
- Burt, T. P., Howden, N. J. K., Worrall, F., & McDonnell, J. J. (2011). On the value of long-term, low-frequency water quality sampling: avoiding throwing the baby out with the bathwater. *Hydrological Processes*, 25, 828-830. <https://doi.org/10.1002/hyp.7961>

- Calleja, M. L., Al-Otaibi, N., & Moran, X. A. G. (2019). Dissolved organic carbon contribution to oxygen respiration in the central Red Sea. *Scientific Reports*, 9, 4690. <https://doi.org/10.1038/s41598-019-40753-w>
- Carr, J., D'Odorico, P., McGlathery, K. J., & Wiberg, P. L. (2012). Modeling the effects of climate change on eelgrass stability and resilience: future scenarios and leading indicators of collapse. *Marine Ecology Progress Series*, 488, 289-301. <https://doi.org/10.3354/meps09556>
- Coraggio, E., Han, D., Gronow, C., & Tryfonas, T. (2022). Water Quality Sampling Frequency Analysis of Surface Freshwater: A Case Study on Bristol Floating Harbour. *Frontiers in Sustainable Cities*, 3, 791595. <https://doi.org/10.3389/frsc.2021.791595>
- Dalley, N. E. (1986). High Frequency Monitoring of a Coastal Stream. *Developments in Water Science*, 27, 433-442. [https://doi.org/10.1016/S0167-5648\(08\)70811-6](https://doi.org/10.1016/S0167-5648(08)70811-6)
- Davis, S. E., Cable, J. E., Childers, D. L., Coronado-Molina, C., Day, J., Hittle, C. D., Madden, C. J., Reyes, E., Rudnick, D., Sklar, F. (2004). Importance of Storm Events in Controlling Ecosystem Structure and Function in a Florida Gulf Coast Estuary. *Journal of Coastal Research*, 204, 1198-1208. <http://dx.doi.org/10.2112/03-0072R.1>
- Emerson, S., Watanabe, Y. W., Ono, T., & Mecking, S. (2004). Temporal Trends in Apparent Oxygen Utilization in the Upper Pycnocline of the North Pacific: 1980-2000. *Journal of Oceanography*, 60, 139-147. <https://doi.org/10.1023/B:JOCE.0000038323.62130.a0>
- Glover, D. M., Jenkins, W. J., & Doney, S. C. (2011). *Modeling Methods for Marine Science*. Cambridge University Press.
- Granger, S. J., Qunicke, J. A., Harris, P., Collins, A. L., & Blackwell, M. S. (2018). Comparison of high frequency, in-situ water quality analysers and sensors with conventional water

sample collection and laboratory analyses: phosphorus and nitrogen species (2018).

*Hydrology and Earth Systems Sciences Discussions* [preprint].

<https://doi.org/10.5194/hess-2017-684>, 2018.

Havens, K. (2018). *Climate Change: Effects on Salinity in Florida's Estuaries and Responses of Oysters, Seagrass, and Other Animal and Plant Life*. UF IFAS Extension. Retrieved May 5, 2022, from <https://edis.ifas.ufl.edu/publication/SG138>.

Hondula K. L. & M. L. Pace (2014). Macroalgal support of cultured hard clams in a low nitrogen coastal lagoon. *Marine Ecology Progress Series*, 498, 187-201.

<https://doi.org/10.3354/meps10644>

Kennedy, V. S. (1990). Anticipated Effects of Climate Change on Estuarine and Coastal Fisheries. *Fisheries*, 15(6), 16-24.

[http://dx.doi.org/10.1002/\(SICI\)1099-1085\(19970630\)11:8%3C949::AID-HYP513%3E3.0.CO;2-G4108254](http://dx.doi.org/10.1002/(SICI)1099-1085(19970630)11:8%3C949::AID-HYP513%3E3.0.CO;2-G4108254)

Kim, H., Takayama, K., Hirose, N., Onitsuka, G., Yoshida, T., & Yanagi, T. (2019). Biological modulation in the seasonal variation of dissolved oxygen concentration in the upper Japan Sea. *Journal of Oceanography*, 75, 257-271.

<https://doi.org/10.1007/s10872-018-0497-6>

Kothandraman, V. & Evans, R. L. (1972). *Use of Air-Water Relationships for Predicting Water Temperature* (Report of Investigation No. 69). State of Illinois Department of Registration and Education.

<https://www.ideals.illinois.edu/bitstream/handle/2142/102011/ISWSRI-69.pdf?sequence=1&isAllowed=y>

- Kuang, C., Dong, Z., Gu, J., Su, T-S, Zhan, H., & Zhao, W. (2020). Quantifying the influence factors on water exchange capacity in a shallow coastal lagoon. *Journal of Hydro-environment Research*, 31, 26-40. <https://doi.org/10.1016/j.jher.2020.03.005>
- Liao, A., Han, D., Song, X., & Yang, S. (2021). Impacts of storm events on chlorophyll-a variations and controlling factors for algal bloom in a river receiving reclaimed water. *Journal of Environmental Management*, 297, 113376. <https://doi.org/10.1016/j.jenvman.2021.113376>
- Liu, J., Wang, B., Oldham, C. E., & Hipsey, M. R. (2020). Unravelling the metabolism black-box in a dynamic wetland environment using a hybrid model framework: Storm driven changes in oxygen budgets. *Science of The Total Environment*, 723, 138020. <https://doi.org/10.1016/j.scitotenv.2020.138020>
- McGlathery, K. J., & Cristian R. R. (2021). Water Quality Sampling- integrated measurements from the Virginia Coast, 1992-2021. Virginia Coast Reserve Long-Term Ecological Research Project Data Publication [knb-lter-vcr.247.14](https://doi.org/10.6073/pasta/db7f8fe720ddfcdfab1352adc9c22702). (doi:10.6073/pasta/db7f8fe720ddfcdfab1352adc9c22702 )
- Mertens, C. (1996). Oxsat.
- Mulholland, P. J., Best, G. R., Coutant, C. C., Hornberger, G. M., Meyer, J. L., Robinson, P. J., Senberg, J. R., Turner, R. E., Vera-Herrera, F., & Wetzel, R. G. (1998). Effects of Climate Change on Freshwater Ecosystems of the South-eastern United States and the Gulf Coast of Mexico. *Hydrological Processes*, 11(8), 949-970. [https://doi.org/10.1002/\(SICI\)1099-1085\(19970630\)11:8<949::AID-HYP513>3.0.CO;2-G](https://doi.org/10.1002/(SICI)1099-1085(19970630)11:8<949::AID-HYP513>3.0.CO;2-G)
- NASA (n.d.). *Highlights*. Accessed March 13, 2023 from <https://salinity.oceansciences.org/highlights08.htm>

- NASA Prediction of Worldwide Energy Resources. *The POWER Project*. Retrieved August 23, 2022. <https://power.larc.nasa.gov/data-access-viewer/>
- National Data Buoy Center (2022). *Station WAHV2- 8631044- Wachapreague, VA*. Accessed August 23, 2022, from [https://www.ndbc.noaa.gov/station\\_page.php?station=wahv2](https://www.ndbc.noaa.gov/station_page.php?station=wahv2)
- National Weather Service (2021). *Storm Data Preparation: National Weather Service Instruction 10-605*. <https://www.nws.noaa.gov/directives/sym/pd01016005curr.pdf>
- Newton, A., Brito, A. C., Icely, J. D., Derolez, V., Clara, I., Angus, S., Schernewski, G., Inacio, M., Lillebo, A. I., Sousa, A. I., Bejaoui, B., Solidoro, C., Tosic, M., Canedo-Arguelles, M., Yamamuro, M., Reizopoulou, S., Tseng, H-C., Canu, D., Roselli, L., Maana, M., Cristiana, S., Ruiz-Fernandez, A. C., de Lima, R. F., Kjerfve, B., Rubio-Cisneros, N., Perez-Ruzafa, A., Marcos, C., Pastres, R., Pranovi, F., Snoussi, M., Turpie, J., Tuchkovenko, Y., Dyack, B., BRookes, J., Povilanskas, R., & Khokhlov, V. (2018). Assessing, quantifying and valuing the ecosystem services of coastal lagoons. *Journal for Nature Conservation*, 44, 50-65. <https://doi.org/10.1016/j.jnc.2018.02.009>
- NOAA (n.d.). *Historical Hurricane Tracks*. Retrieved 25, October 2022, from <https://coast.noaa.gov/hurricanes/#map=4/32/-80>.
- NOAA Tides & Currents (2022). *Wachapreague, VA- Station ID: 8631044*. Retrieved August 23, 2022, from <https://tidesandcurrents.noaa.gov/stationhome.html?id=8631044>.
- Pastres, R., Ciavatta, S., & Solidoro, C. (2003). The Extended Kalman Filter (EKF) as a tool for the assimilation of high frequency water quality data. *Ecological Modelling*, 170(2-3), 227-235. [https://doi.org/10.1016/S0304-3800\(03\)00230-8](https://doi.org/10.1016/S0304-3800(03)00230-8)
- Perez-Ruzafa, A., Campillo, S., Fernandez-Palacios, J. M., Garcia-Lacunza, A., Garcia-Oliva, M., Ibanez, H., Navarro-Martines, P. C., Perez-Marcos, M., Perez-Ruzafa, I. M.,

- Quispe-Becerra, J. I., Sala-Mirete, A., Sanchez, O. & Marcos, C. (2019). Long-Term Dynamic in Nutrients, Chlorophyll a, and Water Quality Parameters in a Coastal Lagoon During a Process of Eutrophication for Decades, a Sudden Break and a Relatively Rapid Recovery. *Frontiers in Marine Science*, 6. <https://doi.org/10.3389/fmars.2019.00026>
- Perna, C. & Burrows, D. (2005). Improved dissolved oxygen status following removal of exotic weed mats in important fish habitat lagoons of the tropical Burdekin River floodplain, Australia. *Marine Pollution Bulletin*, 51(1-4), 138-148.  
<https://doi.org/10.1016/j.marpolbul.2004.10.050>
- Project Description* (n.d.). Virginia Coast Reserve Long Term Ecological-Research Retrieved August 23, 2022, from  
[https://www.vcrlter.virginia.edu/elevol/VCR\\_LTER\\_VII\\_Proposal\\_FINAL\\_Project\\_Description.pdf](https://www.vcrlter.virginia.edu/elevol/VCR_LTER_VII_Proposal_FINAL_Project_Description.pdf)
- Ross, P.G., & Snyder, R. A. (2020). Ecological Monitoring Program at VIMS ESL- Annual Report 2018-2019. Virginia Institute of Marine Science, William & Mary.  
<https://scholarworks.wm.edu/reports/2090>
- Safak, I., Wiberg, P. L., Richardson, D. L., & Kurum, M. O. (2015). Controls on residence time and exchange in a system of shallow coastal bays. *Continental Shelf Research*, 97, 7-20.  
<https://doi.org/10.1016/j.csr.2015.01.009>
- Safak, I., P. Wiberg, and D. Richardson. 2018. Residence time in lagoons on the coast of Virginia, 2002 and 2009 ver 4. Environmental Data Initiative.  
<https://doi.org/10.6073/pasta/e91c86824089544f5d74608bd620e557> (Accessed 2023-04-22).
- Saraceno, J. F., Pellerin, B. A., Downing, B. D., Boss, E., Bachand, P. A. M., & Bergamaschi, B. A. (2009). High-frequency in situ optical measurements during a storm event: Assessing

relationships between dissolved organic matter, sediment concentrations, and hydrologic processes. *Journal of Geophysical Research: Biogeosciences*, 114(G4).

<https://doi.org/10.1029/2009JG000989>

Scanes, P., Coade, G., Doherty, M., & Hill, R. (2007). Evaluation of the utility of water quality based indicators of estuarine lagoon condition in NSW, Australia. *Estuarine, Coastal and Shelf Science*, 74(1-2), 306-319. <https://doi.org/10.1016/j.ecss.2007.04.021>

Searcy, R. T. & Boehm, A. B. (2021). A Day at the Beach: Enabling Coastal Water Quality Prediction with High-Frequency Sampling and Data-Driven Models. *Environmental Science Technology*, 55(3), 1908-1918. <https://doi.org/10.1021/acs.est.0c06742>

Sefan, H. G. & Preud'Homme, E. B. (1993). Stream Temperature Estimation from Air Temperature. *Journal of the American Water Resources Association*, 29(1), 27-45.

<https://doi.org/10.1111/j.1752-1688.1993.tb01502.x>

Taboga, Marco (2021). *Lectures on probability theory and mathematics statistics*. Kindle Direct Publishing.

Trombetta, T., Vidussi, F., Mas, S., Parin, D., Simier, M., & Mostajir, B. (2019). Water temperature drives phytoplankton blooms in coastal waters. *PLOS One*, 14(4), e0214933, <https://doi.org/10.1371/journal.pone.0214933>

VIMS ESL (2022). *ESL Water Quality Monitoring*. Accessed 11 December 2022 from [https://www.vims.edu/esl/research/water\\_quality/](https://www.vims.edu/esl/research/water_quality/).

Wilks, D. S. (2011). *Statistical Methods in the Atmospheric Sciences* (3rd ed.). Elsevier.

Yu, S. J., Ryu, I. G., Park, M. J., & Im, J. K. (2021). Long-term relationship between air and water temperatures in Lake Paldang, South Korea. *Environmental Engineering Research*, 26(4), 200177. <https://doi.org/10.4491/eer.2020.177>

Yuan, X., Yin, K., Harrison, P. J., He, L., & Xu, J. (2011). Variations in Apparent Oxygen Utilization and Effects of P Addition on Bacterial Respiration in Subtropical Hong Kong Waters. *Estuaries and Coasts*, 34(3), 536-543.

<https://doi.org/10.1007/s12237-010-9329-7>